Utjecaj karakteristika vjetra na prirodnu ventilaciju zgrada

Miše, Dino

Undergraduate thesis / Završni rad

2019

Degree Grantor / Ustanova koja je dodijelila akademski / stručni stupanj: **University of Zagreb, Faculty of Mechanical Engineering and Naval Architecture / Sveučilište u Zagrebu, Fakultet strojarstva i brodogradnje**

Permanent link / Trajna poveznica: https://urn.nsk.hr/urn:nbn:hr:235:256215

Rights / Prava: In copyright/Zaštićeno autorskim pravom.

Download date / Datum preuzimanja: **2024-05-02**

Repository / Repozitorij:

Repository of Faculty of Mechanical Engineering and Naval Architecture University of Zagreb

Univeristy of Zagreb

Faculty of Mechanical Engineering and Naval Architecture

BACHELOR'S THESIS

Dino Miše

Zagreb, 2019.

UNIVERSITY OF ZAGREB

FACULTY OF MECHANICAL ENGINEERING AND NAVAL
ARCHITECTURE

EFFECTS OF WIND CHARACTERISTICS ON NATURAL VENTILATION OF BUILDINGS

Mentors:

Prof. Hrvoje Kozmar, PhD

Ass. Prof. Walter Meile, PhD

Student:

Dino Miše

ZAGREB, 2019.

Statement | Izjava

I hereby declare that I have made this thesis independently using the knowledge acquired during my studies and the cited references.

Izjavljujem da sam ovaj rad radio samostalno koristeći znanja stečena tijekom studija i navedenu literaturu.

Zagreb, February 2019.   Dino Miše

SVEUČILIŠTE U ZAGREBU
FAKULTET STROJARSTVA I BRODOGRADNJE
Središnje povjerenstvo za završne i diplomske ispite
Povjerenstvo za završne ispite studija strojarstva za smjerove:
procesno-energetski, konstrukcijski, brodostrojarski i inženjersko modeliranje i računalne simulacije

Sveučilište u Zagrebu	
Fakultet strojarstva i brodogradnje	
Datum	Prilog
Klasa:	
Ur.broj:	

ZAVRŠNI ZADATAK

Student: **Dino Miše**   Mat. br.: **0035204303**

Naslov rada na
hrvatskom jeziku: **Utjecaj karakteristika vjetra na prirodnu ventilaciju zgrada**

Naslov rada na
engleskom jeziku: **Effects of wind characteristics on natural ventilation of buildings**

Opis zadatka:

Natural ventilation of buildings is important for a good indoor air quality. The basic ventilation parameter is the air change rate (ACH), which represents the air removed from an indoor space divided by the indoor space volume. The ACH strongly depends on wind characteristics in the lower atmosphere, as well as on the openness of building doors and windows.

Small-scale experiments will be conducted in a boundary layer wind tunnel of the Institute of Fluid Mechanics and Heat Transfer at the Graz University of Technology, Austria. The cubic building model with single and double window openings will be studied in a stand-alone configuration as well as a part of an urban neighborhood. The cubic building model will be subjected to the rural and suburban atmospheric boundary layers simulations to investigate the effects of inflow wind characteristics on the ACH of the studied building at various flow incidence angles.

In this thesis, it is necessary to provide:

1) Introduction including theoretical background on aerodynamics of buildings and their natural ventilation;
2) Experimental setup including details of the wind-tunnel design, simulation of the atmospheric boundary layers, experimental technique and procedure;
3) Results and discussion;
4) Conclusions.

The advice is to list references used in this work, as well as to acknowledge help and support received during this study.

Zadatak zadan: Rok predaje rada: Predviđeni datumi obrane:
                              1. rok: 22. veljače 2019.   **1. rok:** 25.2. - 1.3. 2019.
29. studenog 2018.   **2. rok (izvanredni):** 28. lipnja 2019.   **2. rok (izvanredni):** 2.7. 2019.
                              3. rok: 20. rujna 2019.   **3. rok:** 23.9. - 27.9. 2019.

Zadatak zadao: Predsjednik Povjerenstva:

Prof. dr. sc. Hrvoje Kozmar

Ass. Prof. Dr. techn. Walter Meile   Prof. dr. sc. Igor Balen

Contents

List of Figures

List of Tables

List of Symbols

Greek symbols

Abbrevatons

Sažetak

Prirodna ventilacija je proces dobave svježeg zraka u zatvoreni prostor i uklanjanje ustajalog zraka iz prostorije bez rada mehaničkog uređaja. Za izmjenu zraka koriste se prirodne sile gibanja zraka i uzgona. U vrijeme sve veće potrošnje električne energije i zagađenja okoliša, ovaj ekološki prihvatljiv način izmjene zraka je vrlo poželjan. Za iskorištavanje punog potencijala prirodne izmjene zraka i konstrukciju uređaja koji će je pospješiti, važno je poznavati karakteristike parametara koji utječu na efikasnost ventilacije. S ciljem detaljnijeg analiziranja parametara koji utječu na prirodnu ventilaciju zgrada su provedeni modelski eksperimenti u zračnom tunelu za generiranje modela atmosferskog graničnog sloja na Institutu za mehaniku fluida i prijenos topline Tehničkog sveučilišta u Grazu, Austrija. Cilj istraživanja bio je odrediti utjecaj karakteristika vjetra na intenzitet prirodne ventilacije samostalne zgrade, kao i one smještene u urbanom okruženju, i to za atmosferski granični sloj modeliran za strujanje nad ruralnim i prigradskim terenom. Karakteristike strujanja zraka su određene na temelju mjerenja brzine sustavom užarene žice, a za izmjenu zraka u modelu zgrade je korišten sustav praćenja koncentracije plina. Ispitivanje je provedeno za jednostranu i poprečnu ventilaciju modela zgrade, pri čemu se na modelu zgrade nalazio jedan odnosno dva prozora, mijenjajući brzinu i kut nastrujavanja zraka i udaljenost među modelima zgrada. Za oba je modela atmosferskog graničnog sloja izmjena zraka veća prilikom poprečnog nastrujavanja zraka i raste s porastom brzine. Također, izmjena zraka je prilikom poprečnog nastrujavanja intenzivnija ako je model zgrade samostalan, tj. ako nije dio urbanog naselja.

Ključne riječi: atmosferski granični sloj, prirodna ventilacija, turbulencija, ruralni teren, prigradski teren, eksperimenti u zračnom tunelu

Summary

Natural ventilation is a process of supplying the fresh air in the indoor space and removing the saturated air from the indoor space without using a mechanical device. The driving forces for this air exchange are the buoyancy and the flow momentum. At a time of increasing electrical consumption and environmental pollution, it is important to promote this environmentally friendly technology. To exploit its full potential, it is necessary to properly understand the relationship between parameters that affect its efficiency. Therefore, small-scale model experiments were carried out in a boundary layer wind tunnel at the Institute of Fluid Mechanics and Heat Transfer at the Graz University of Technology, Austria. It was attempted to determine the influence of inflow characteristics on the characteristics of a natural ventilation of a stand-alone cubic building as well as of a building situated in an urban environment. The atmospheric boundary layer was successfully modeled to simulate flow over rural and suburban terrain types. A hot-wire anemometry system was used to measure turbulent flow characteristics, while tracer gas system was employed to determine air exchange rates. Experiments were conducted for single-side and cross-ventilation arrangements of the studied building model. The analyzed parameters include the flow velocity and its incidence angle as well as a distance between the buildings. The experimental results indicate that the natural ventilation has similar patterns for both studied atmospheric boundary layer models, whereas the rural-type atmospheric boundary layer model is more sensitive to the changes of input parameters. Air change rate is larger for larger wind velocities, as well as for cross-ventilated buildings compared to the single-side ventilation arrangement.

Keywords: atmospheric boundary layer, natural ventilation, turbulence, rural terrain, suburban terrain, wind tunnel experiment

Prošireni sažetak

Uvod

Prirodna ventilacija je najčešće korišteni način izmjene zraka u zatvorenim prostorima. Za dobavu svježeg zraka koristi prirodne sile razlike tlaka i uzgona. Osim besplatnom pogonskom energijom, ovaj se način izmjene zraka ističe ekološkom prihvatljivošću i malim investicijskim troškovima. Poznavanje karakteristika parametara prirodne ventilacije neophodno je za projektiranje kvalitetnog sustava.

Utjecaj okolnih zgrada, njihov raspored i gustoća te kut i brzina nastrujavanja vjetra poznati su parametri koji uvjetuju intenzitet izmjene zraka. Međutim, u prethodnim je istraživanjima malo pažnje posvećeno karakteristikama vjetra unutar atmosferskog graničnog sloja s obzirom na teren preko kojeg zrak struji. Upravo je taj parameter detaljnije obrađen u ovome radu.

Mjerena je količina izmijenjenog zraka samostalnog modela zgrade smještenog na ruralnoj i prigradskoj vrsti terena. Ispitivanje je provedeno za jednostranu i poprečnu ventilaciju zgrade. Zatim je oko ispitnog modela postavljeno osam identičnih modela zgrade kako bi se simulirali uvjeti naseljene četvrti i sva mjerenja su ponovljena za tri različite gustoće modela zgrada.

Atmosferski granični sloj

Zemljina atmosfera sastoji se od niza slojeva. Za područje industrijske aerodinamike najznačajniji je najniži sloj - troposfera. Preciznije njen donji dio koji se naziva atmosferski granični sloj (ABL). Brzina u atmosferskom graničnom sloju raste od nule u dodiru s tlom do brzine neporemećenog strujanja na njegovom rubu δ. Unutarnji dio ABL-a prostire se kroz donjih $10 - 15\%$ visine δ. U njemu je strujanje pod utjecajem karakteristika terena. Vanjski dio nastavlja se do visine $\delta = $ 450-600 m, a dominantan je utjecaj Coriolisove sile uslijed rotacije Zemlje, slika 0.1.
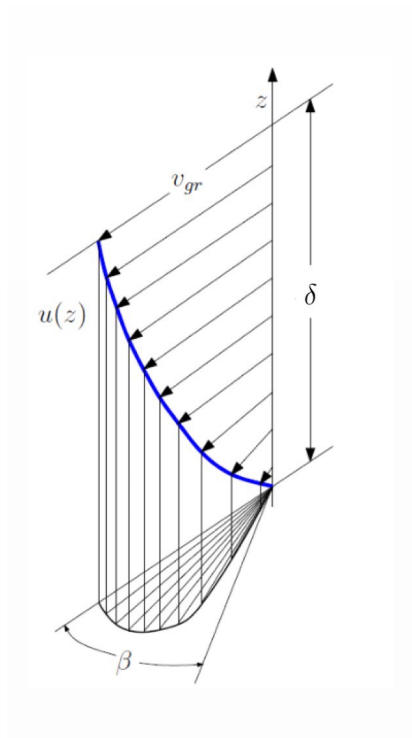
Slika 0.1: Profil brzine unutar atmosferskog graničnog sloja, [1]

Unutar atmosferskog graničnog sloja strujanje je turbulentno. Karakteristike strujanja koje opisuju atmosferski granični sloj su srednja brzina strujanja zraka, intenzitet turbulencije, integralna duljinska mjera turbulencije, Reynoldsovo naprezanje i spektar kinetičke energije turbulentnih pulzacija brzine.

Eksperimentalne postavke

Atmosferski granični sloj je modeliran za strujanje iznad ruralnog i prigradskog tipa terena u zračnom tunelu za generiranje modela atmosferskog graničnog sloja na Institutu za mehaniku fluida i prijenos topline Tehničkog sveučilišta u Grazu, Austrija. Zračni tunel je tipa Göttingen i zatvorenog je sustava rada. Za simulaciju graničnog sloja u mjernu je sekciju umetnuta rešetka s nepravilnim rasporedom cilindričnih cijevi, nazubljena barijera i podna hrapavost. Na slici 0.2 prikazana je mjerna sekcija na čijem se kraju nalazi konfiguracija urbane četvrti. Izmjena je zraka ispitivana na središnjem modelu s dva poprečna prozora. U slučaju ispitivanja jednostrane ventilacije jedan je prozor zabrtvljen poklopcem.

Slika 0.2: Shema sastavnih dijelova ispitne sekcije IFMHT-GUT zračnog tunela, dimenzije u mm

Učinkovitost ventilacije opisuje se brojem izmjena zraka (ACH) u jednom satu: $\text{ACH} = \frac{\dot{V}}{V_R}$, gdje je V_R volumen promatrane prostorije, a $\dot{V}$ volumni protok. ACH je izračunat iz podataka dobivenih sustavom za praćenje koncentracije plina za samostalni model zgrade i za model zgrade kao dio naseljene četvrti sa:

a)   Malom udaljenost između modela, $d = 0.5a$,

b)   Srednjom udaljenost između modela, $d = a$,

c)   Velikom udaljenost između modela, $d = 1.5a$,

gdje je a dužina brida modela ($a = 200$ mm). Mjerenja brzine provedena su anemometrom kojemu je osjetnik užarena žica konstantne temperature.

Rezultati i zaključak

Dobiveni su profili brzine za strujanje u ruralnom i prigradskom atmosferskom graničnom sloju uspoređeni sa zakonom potencije i logaritamskim zakonom na slici 0.3.
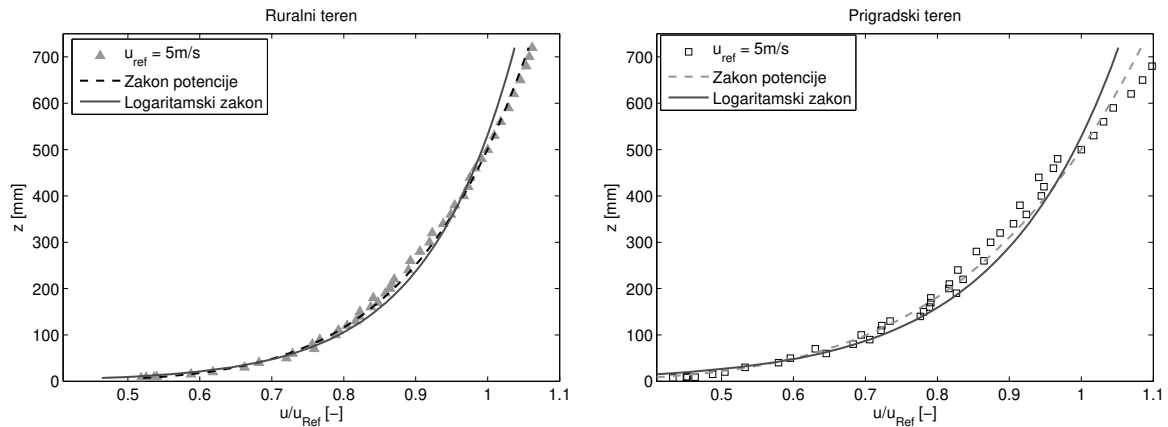
Slika 0.3: Profili osrednjene brzine za ruralni i prigradski tip terena uspoređeni sa zakonom potencije i logaritamskim zakonom

Nakon prikaza profila osrednjene brzine obrađeni su podaci za karakteristike turbulencije. Na slikama 0.4 i 0.5 prikazani su rezultati integralne duljinske mjere turbulencije i spektralne raspodjele kinetičke energije turbulencije za obje vrste terena.
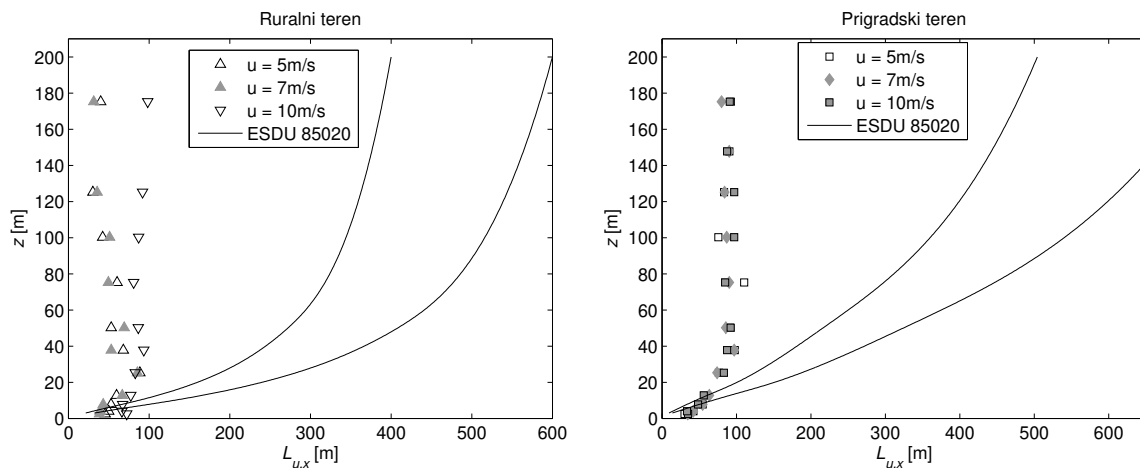
Slika 0.4: Integralna duljinska mjera turbulencije i pripadajuće vrijednosti ESDU 85020 standarda
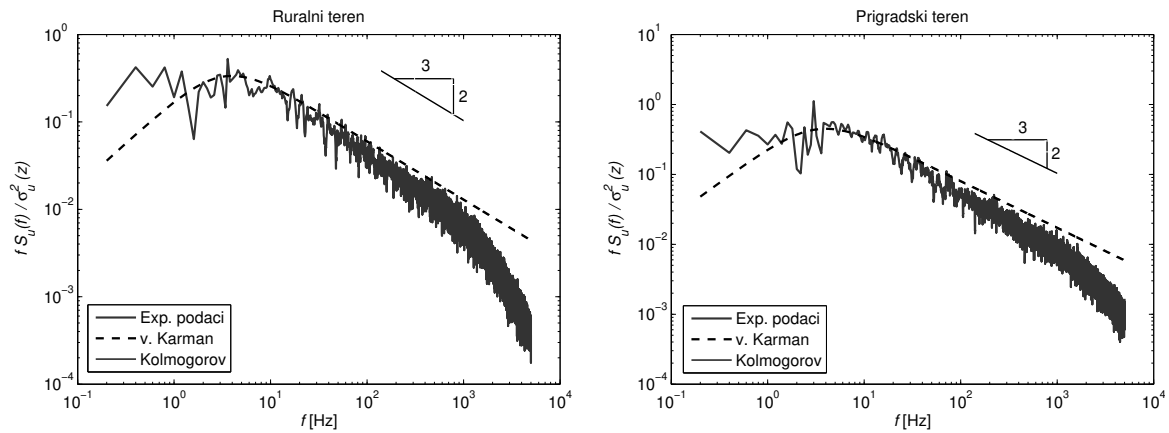
Slika 0.5: Usporedba spektralne raspodjele kinetičke energije turbulencije s teorijskim modelima von Kármána i Kolmogorova

Drugi dio ispitivanja sastojao se od mjerenje broja izmjena zraka u jednom satu. Rezultati za samostalnu zgradu u ovisnosti o kutu nastrujavanja i brzini dani su na slici 0.6.
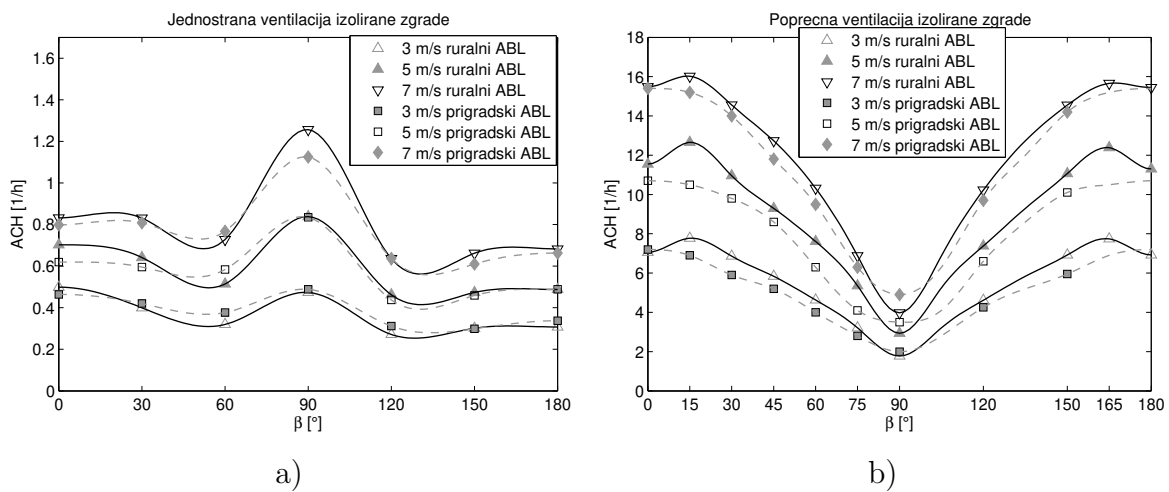
Slika 0.6: Ovisnost broja izmjena zraka o kutu nastrujavanja i brzini za samostalnu zgradu, a) jednostrana ventilacija, b) poprečna ventilacija

Slika 0.7 prikazuje ovisnost broja izmjena zraka o kutu nastrujavanja i gustoći okolnih zgrada za jednostranu ventilaciju pri konstantnoj brzini nastrujavanja (5 m/s). Ista je ovisnost, ali za poprečno prostrujavanje prikazana na slici 0.8.

a)   b)
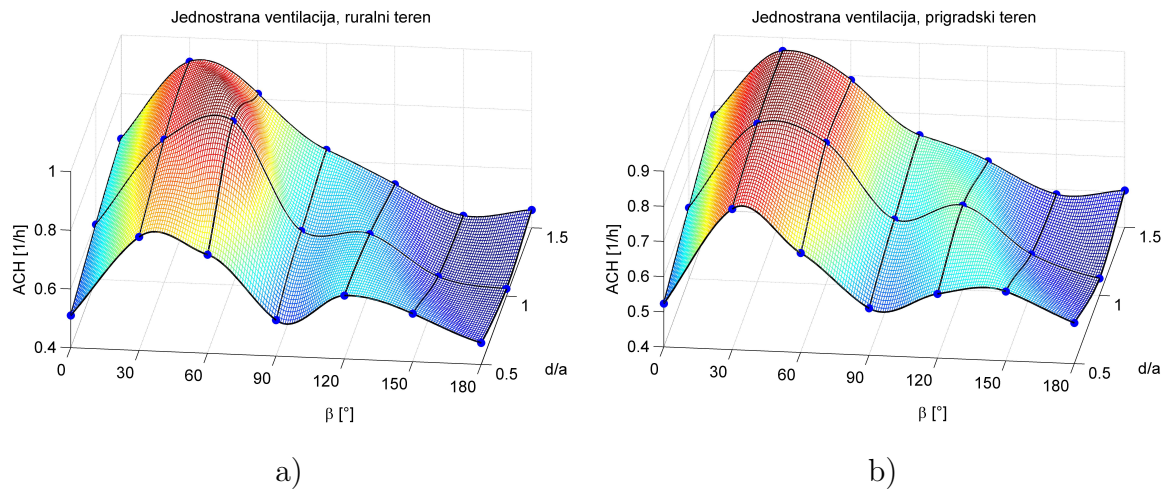
Slika 0.7: Ovisnost broja izmjena zraka o kutu nastrujavanja i gustoći raspodjele okolnih zgrada za jednostranu ventilaciju pri brzini nastrujavanja $u = 5$ m/s, a) ruralni teren, b) prigradski teren

a)   b)
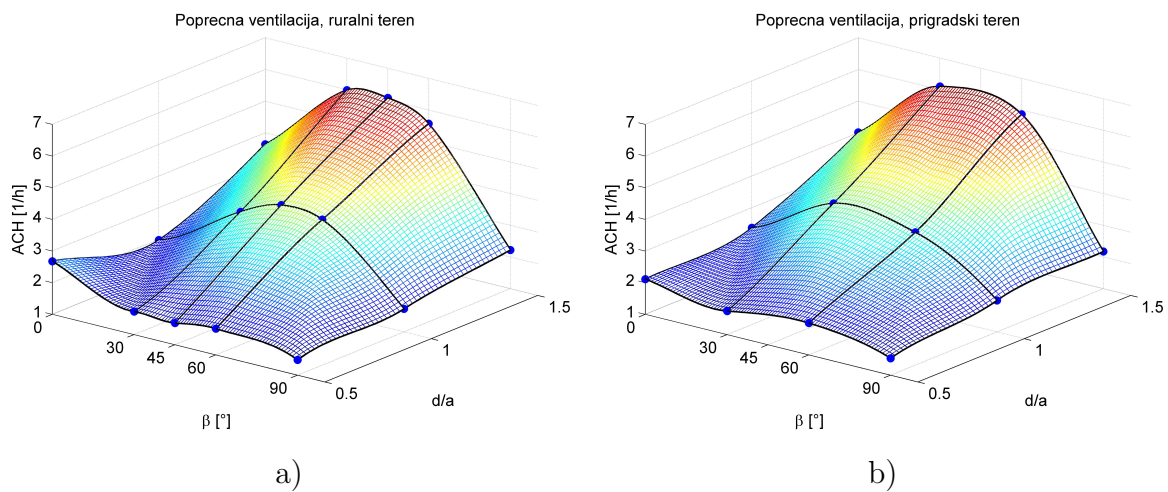
Slika 0.8: Ovisnost broja izmjena zraka o kutu nastrujavanja i gustoći raspodjele okolnih zgrada za poprečnu ventilaciju pri brzini nastrujavanja $u = 5$ m/s, a) ruralni teren, b) prigradski teren

U zračnom su tunelu uspješno modelirani atmosferski granični slojevi karakteristični za ruralno i prigradsko područje. Dobivene su ciljane vrijednosti eksponenata zakona potencije $\alpha = 0.15$ za ruralno i 0.22 za prigradsko područje. Izračunate vrijednosti aerodinamičke duljine hrapavosti svedene na prirodnu veličinu se podudaraju s međunarodnim ESDU standardom. Integralne duljinske mjere turbulencije su manje od ESDU vrijednosti, što je uobičajeno za simulacije u zračnom tunelu. Zidovi zračnog tunela ne dopuštaju razvijanje velikih vrtloga. Spektar raspodjele kinetičke energije turbulencije prati teorijske modele von Kármána i Kolmogorova. Dobiveni je intenzitet turbulencije manji u odnosu na vrijednosti u ESDU standardu, a Reynoldsovo naprezanje jasno prati prirodne zakone.

Trendovi i vrijednosti broja izmjena zraka ruralnog i prigradskog atmosferskog graničnog sloja u ovisnosti o kutu i brzini nastrujavanja, kao i gustoći okolnih zgrada, prilično su slični. Oba modela atmosferskog graničnog sloja postižu maksimum kod jednostrane ventilacije samostalne zgrade za $\beta = 90°$. U slučaju poprečnog nastrujavanja izolirane zgrade maksimum se za prigradski sloj postiže pri $\beta = 0°$, dok je za prigradski sloj on kod $\beta = 15°$. Ventilacija zgrade koja čini dio naselja najintenzivnija je za kuteve nastrujavanja između $\beta = 30°$ i $60°$ i raste s povečanjem brzine. Smanjenjem gustoće zgrada unutar naseljenog područja povećava se ACH kod poprečne ventilacije. Izuzetak je kut od $\beta = 0°$ za ruralno naselje. Jednostrana ventilacija ne prati tu zakonitost. Kod nje utjecaj okolnih zgrada može biti i pozitivan tako što stvoreno polje tlaka uslijed većih brzina strujanja u prostoru između zgrada intenzivnije usisava zrak iz prostorije.

1 | Introduction

Nowadays, ventilation is one of the key issues in the building design as it yields thermal comfort and good air quality. Most of the buildings are still ventilated naturally. Natural ventilation is a process of supplying the air in the indoor spaces and removing the saturated air without using mechanical devices. This passive method of cooling is quite attractive as it saves the energy and the environment.

Natural ventilation uses freely available resources of energy. There are two basic types of building natural ventilation, i.e. (a) wind-driven ventilation due to the air pressure difference around a building, (b) thermally induced ventilation due to a difference in temperature inside and outside of a building. In both cases, the flow enters the building through windows, doors or openings in the building envelope and circulates through the interior space. Air change rate (ACH) is a measure that represents the volume of ambient air which enters the building in a certain time divided by the volume of the respective indoor space. A uniform air change rate is essential to improve human comfort and health in the buildings. Full-scale and small-scale wind-tunnel experiments as well as computational simulations are common methods of studying the building natural ventilation. Computational simulations have been often performed to investigate a potential of natural single-side (Allocca [2]) and cross ventilation (Stavrakakis [3]). The full-scale experiments are commonly used to validate the experimental and computational models. In the wind-tunnel experiment, Ernest et al. [4] found correlations of indoor air motion as a function of the wind direction and the external pressure distribution on the facades. Most studies were performed only with respect to stand-alone buildings despite the fact that the proximity to other buildings is likely to yield sub-

stantial effects. In particular, a presence of neighbouring buildings, their arrangement, and spacing density, may also have a significant effect on the local flow field and hence the ventilation characteristics of a studied building, e.g. Cheung and Liu [5] and Lee at al. [6]. Langensteiner [1] studied the building natural ventilation in the suburban environment both for thermally and wind-driven ventilation as well as their interaction.

The present thesis focuses on the ACH of a cubic body that represents a cubic building. The effects of building displacement, flow incidence angle and characteristics were previously not studied as thoroughly as it is the case in this work. The small-scale wind-tunnel simulations were carried out in the IFMHT boundary layer wind tunnel for the rural and the suburban flow conditions. The measurements were performed for a stand-alone building model with one window open (single-side ventilation) first, and subsequerntly for a building model surrounded by dummy objects representing other buildings in a 3 x 3 square pattern. The experiments were performed for the cross-ventilation arrangement of a building model as well. The thermally-induced airflow was out of the scope of the present work that focuses solely on the wind-driven building ventilation.

2 | Theoretical background

2.1. Characteristics of the atmospheric airflow

Just about every wind on Earth can be traced in cause back to the Sun. As the Earth is affected unevenly by heat energy from the Sun, the characteristics of the airflows (winds) are different in different world regions. As a result of this uneven heating, air above the underlying surfaces characterized by higher temperatures will rise due to the buoyancy. On the other hand, the air in contact with the colder surface will sink. Those flow phenomena substantially influence pressure fields in the lower atmosphere and thus the wind characteristics. The rise of the pressure gradient enhances the air flow from the higher to the lower pressure fields. Different patterns of motion, mutually independent in space and time, create atmospheric motions. Figure 2.1 shows an entire range of these phenomena presented as microscale, convective-scale, and macroscale [7].
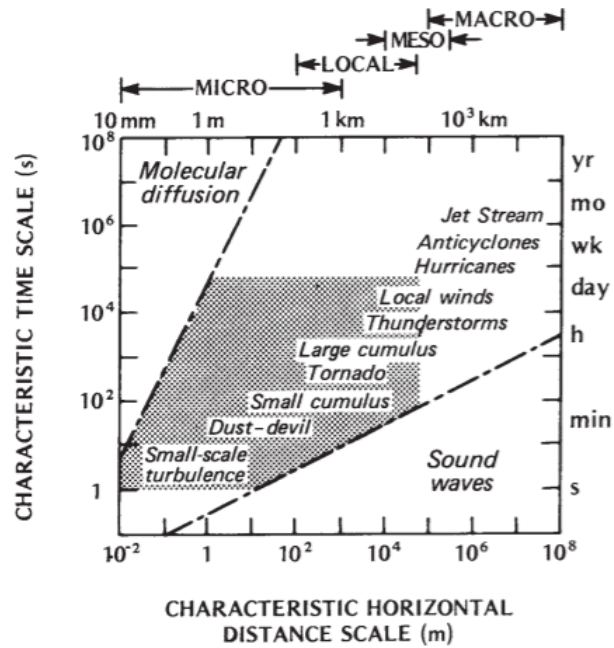
Figure 2.1: Time and space scales of various atmospheric flow phenomena

The atmospheric turbulence generally consists of small vortices with the shortest lifetime (below 10 min) and the size of just a few centimetres to the jet streams determined by large-scale pressure differences that can last for a month and circumvent the entire globe. Elementary air mass moves under the action of forces in the horizontal and vertical directions. Movement in vertical direction caused by a buoyancy force can be equal to 0, act upwards or downwards. According to the direction of this movement, the thermal stratification of the atmosphere may be neutral, unstable or stable. Variation of speed with the hight for different atmospheric stratifications is shown in Fig. 2.2. In the present thesis, the thermal
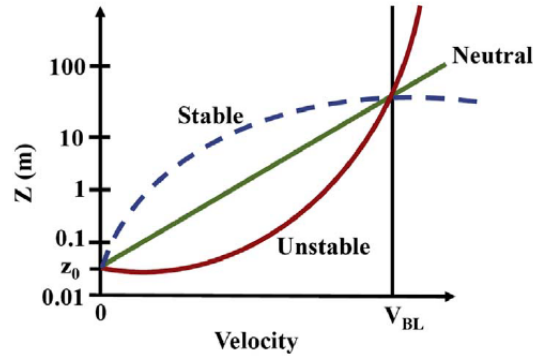
Figure 2.2: Wind profile in the stable, neutral and unstable atmosphere [8]

stratification of the atmosphere is assumed neutral and the mean velocity profile follows the logarithmic law.

In addition to the vertical buoyancy, there are other forces that act horizontally on the air mass.
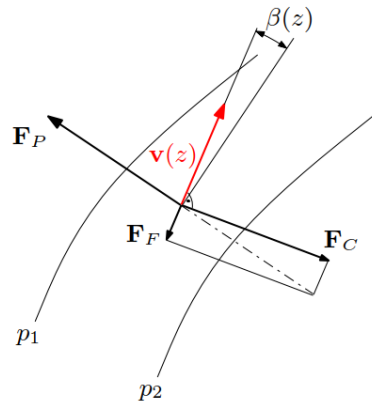
Figure 2.3: Equilibrium of forces in the atmospheric boundary layer [9]

First of them is the horizontal pressure gradient force due to a difference in the air pressure. The lines connecting the points of equal atmospheric pressure are called isobars. In Fig. 2.3 two isobar lines are marked ($p_1 < p_2$). The pressure gradient force is denoted $\vec{F_p}$ and its specific value is:

$$\vec{f_p} = -\frac{1}{\rho}\frac{dp}{dn} \; . \tag{2.1}$$

The Coriolis force develops due to the Earth rotation and it deflects the air parcells moving through the atmosphere. As we are rotating on the Earth only the relative motion of the atmosphere can be noticed. The observer can see that the objects on the Earth have an additional rotational movement. That deviation may be attributed to the Coriolis force:

$$\vec{F_c} = mf\vec{v}, \tag{2.2}$$

From Eq. (2.2) it is evident that the Coriolis force is proportional to the mass of the moving particle (m), its velocity vector ($\vec{v}$ and the Coriolis parameter $f = 2\omega \sin \phi$. The angular velocity vector of the Earth ω is equal to $0.7272 \cdot 10^{-4}$, and the latitude angle is denoted by ϕ. Another force, caused by the momentum transfer between the ground surface and the air appears and constrains the air motion. The impact of this viscous force $\vec{F_f}$ is at the maximum close to the ground and decreases with increasing the height. Directions of the viscous force and air movement are the opposite. The equilibrium of forces driving the flow in the lower atmosphere is illustrated in Fig. 2.3.
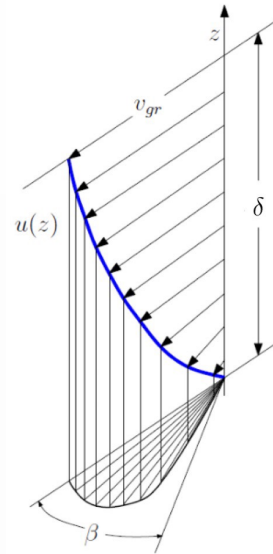
Figure 2.4: Schematic view of the twisted velocity profile in the atmospheric boundary layer [1]

Height at which the influence of viscous forces is negligible is the gradient height (δ). The height range between δ and the ground surface is the atmospheric boundary layer (ABL). The flow velocity on the ground surface is zero (no-slip condition) and it increases to the velocity of the undisturbed flow at the gradient height (upper ABL boundary). According to Dyrbye and Hansen [10] wind direction may vary between $10°$ and $45°$ from the ABL top to the ground surface depending on the atmospheric stability and ground roughness. This phenomenon is combined due to the viscous and Coriolis force effects. This is graphically presented in Fig. 2.4 with the Ekman spiral and β the maximal flow deflection angle.

2.2.   Atmospheric layers

The atmospheric layers are graphically presented in Figs. 2.5 and 2.6.
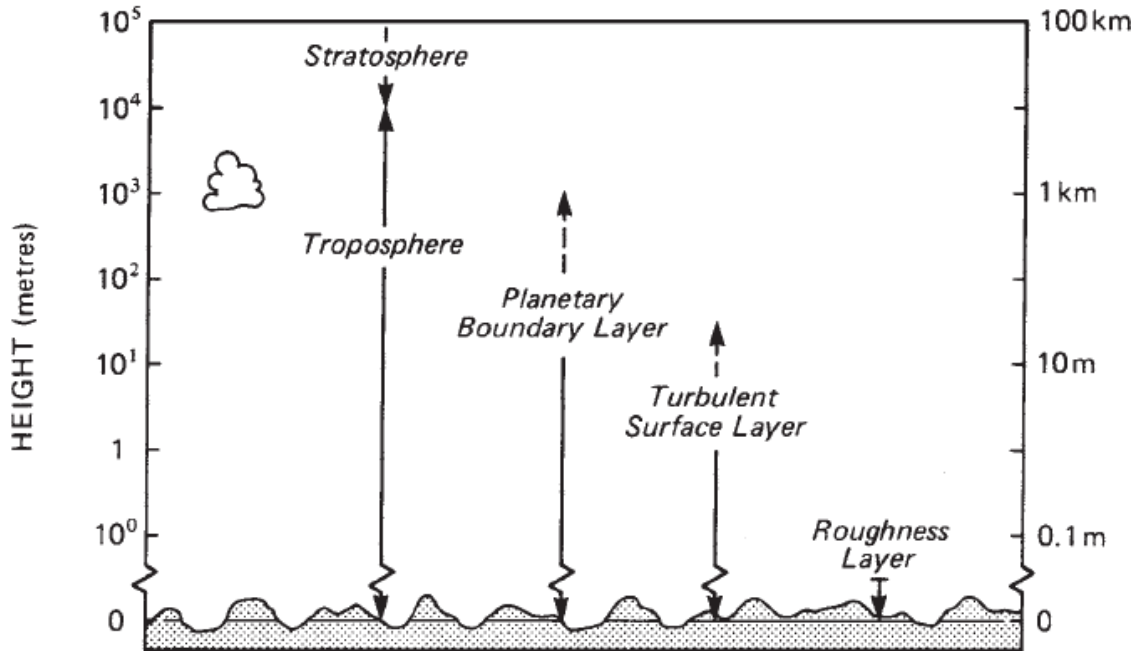
Figure 2.5: The layers of the atmosphere [10]

The Earth atmosphere has a series of layers, each with its specific characteristics. For the subject of this thesis, the lowest layer - troposphere is of a particular importance. More precisely, its bottom part named the atmospheric boundary layer (ABL). Also known as the planetary boundary layer (PBL), it is influenced directly by the presence

of the Earth surface. Its characteristic length scales are vertical and horizontal distances of ~ 1 km and ~ 50 km, respectively, and a characteristic time period of ~ 1 day.

Viscous sublayer also known as roughness sublayer is the lowest and smallest one in touch with the ground where the viscous forces are dominant. In the roughness layer the air motion is controlled by surface roughness. Its depth is dependant upon the dimensions of the surface roughness elements. It extends above the rooftops of buildings and other engineering structures to at least 1 to 3 times their height or spacing. In this zone, the flow is highly irregular as strongly affected by the nature of the individual roughness features, e.g. trees, buildings, etc., [10], [11].

The turbulent surface layer (Prandtl constant-flux layer) is the lower ABL part characterized by intense small-scale turbulence generated by the surface roughness and convection. Despite its variability in the short term (e.g. seconds), the surface layer is horizontally homogeneous when observed over longer periods (longer than 10 min); its thickness is 10-15% of the ABL thickness (up to 100 m above the ground surface). The dominant mechanism of energy, mass and momentum transfer is turbulent stress. In the surface layer, the Coriolis force can still be considered negligible.

From the top of the Prandtl layer to about one kilometre above the surface there is the Ekman layer that covers the largest part of the ABL. The Coriolis effect increases with height untill the top of the ABL where the free atmospheric flow further develops.
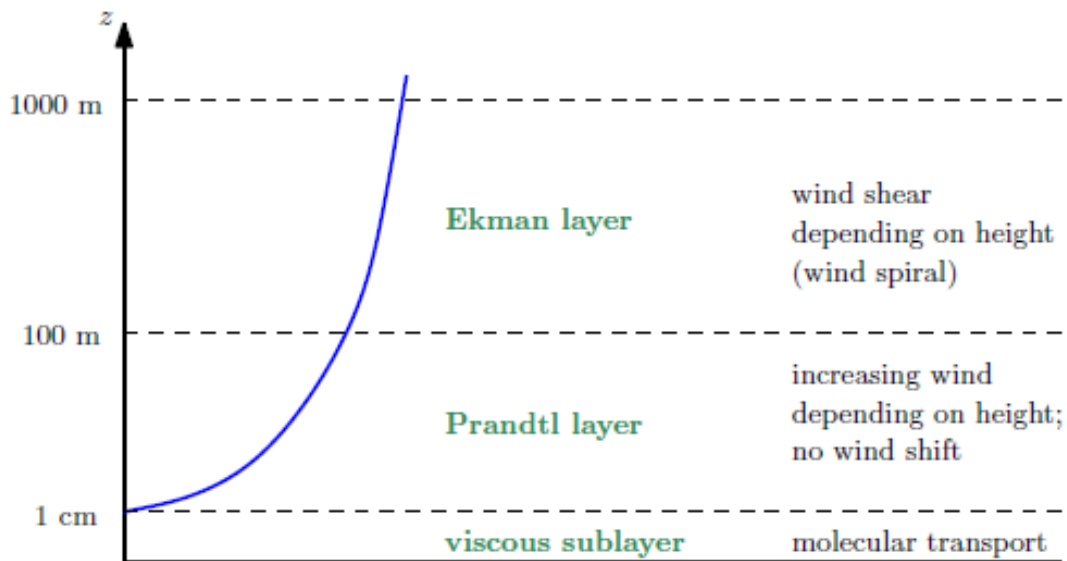
Figure 2.6: Zones within the atmospheric boundary layer [10]

2.3.   Mean velocity characteristics

The atmospheric wind motions are always turbulent. A commonly used concept to describe turbulent flows is to separate absolute velocity into the mean value denoted by an overbar and the fluctuation denoted by a prime:

$$u(t) = \overline{u} + u'(t)$$
$$v(t) = \overline{v} + v'(t) \tag{2.3}$$
$$w(t) = \overline{w} + w'(t).$$

This procedure is known as the Reynolds decomposition. Mean value is averaged over time periods T:

$$\overline{u} = \frac{1}{T} \int_{-T/2}^{T/2} u(t) \mathrm{d}t. \tag{2.4}$$

The turbulent wind velocity time record is shown in Fig. 2.7. The longitudinal velocity component u is considerably larger than the lateral v and vertical w one, so the latter two components may be neglected in the wind-tunnel measurements.
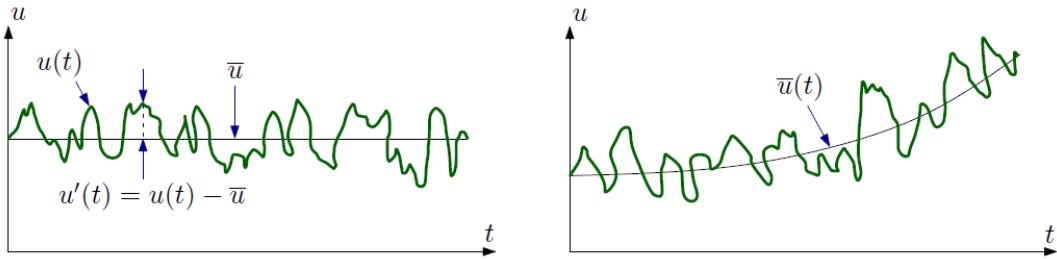
Figure 2.7: Representation of the absolute flow velocity for a certain point in a flow field as well as its mean and fluctuation components [1]

For engineering applications, it is useful to characterize the wind velocity profile, where the mean flow velocity increases with increasing the height from the ground surface. In the lower ABL, up to approximately 100 m, it is possible to use the logarithmic law [12]:

$$\frac{\overline{u}_z}{u_\tau} = \frac{1}{\kappa} \ln \frac{z - d}{z_0}, \tag{2.5}$$

where $\overline{u}_z$ is the mean longitudinal velocity at the height z, u_τ is friction velocity calculated as a square root of the shear stress through density $\sqrt{\dfrac{\tau}{\rho}}$, κ is von Kármán constant equal to 0.4, d is the displacement height and z_0 is the aerodynamic surface roughness length. If we observe the velocity profile in the area of complex flows that develop in-between densely spaced obstacles (e.g. inside city centre, forest or mountains), the zero plane of the mean velocity profile must be raised for the displacement height, which is between 75% [13] and 100% [14] of the surrounding obstacles' height. Aerodynamic surface roughness length is, in theory, equivalent to the height at which the wind velocity becomes zero. Specific values of z_0 are given in Fig. 2.9 and Table 2.1.
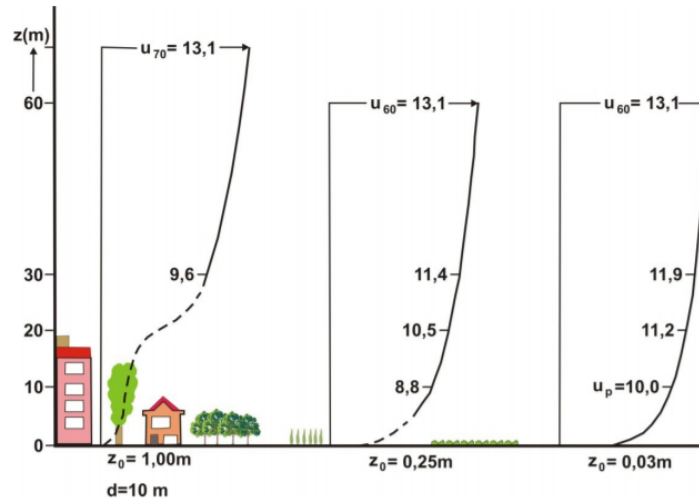
Figure 2.8: Representation of displacement height and aerodynamic surface roughness length [15]

Table 2.1: Classification of the effective terrain roughness according to Wieringa et. al. [16].

Class	z_0 (m)	Landscape description
1. Sea	0.00002	Open sea or lake, tidal flat, snow-covered flat plain, featureless desert, tarmac and concrete with a free fetch of several kilometres.
2. Smooth	0.005	Featureless land surface without any noticeable obstacles and with negligible vegetation; e.g. beaches, pack ice without large ridges, marsh or open country.
3. Open	0.03	Level country with low vegetation (e.g. grass) and isolated obstacles with separations of at least 50 obstacle heights; grazing land without wind breaks, heather, moor and tundra, runway area of airports. Ice with ridges across-wind.
4. Roughly open	0.1	Cultivated or natural area with low crops or plant covers, or moderately open country with occasional obstacles (e.g. low hedges, isolated low buildings or trees) at relative horizontal distances of at least 20 obstacle heights.
5. Rough	0.25	Cultivated or natural area with high crops or crops of varying height, and scattered obstacles at relative distances of 12–15 obstacle heights for porous objects (e.g. shelterbelts) or 8–12 obstacle heights for low solid objects (e.g. buildings).
6. Very rough	0.5	Intensively cultivated landscape with many rather large obstacle groups (large farms, clumps of forest) separated by open spaces of about eight obstacle heights. Low densely planted major vegetation like bush land, orchards, forest. Also, area moderately covered by low buildings with interspaces of three to seven building heights.
7. Skimming	1.0	Landscape regularly covered with similar-size large obstacles, with open spaces of the same order of magnitude as obstacle heights; e.g. mature regular forests, densely built-up area without much building height variation.
8. Chaotic	$2.0 < 8.0$	City centres with mixture of low-rise and high-rise buildings, or large forests of irregular height with many clearings.
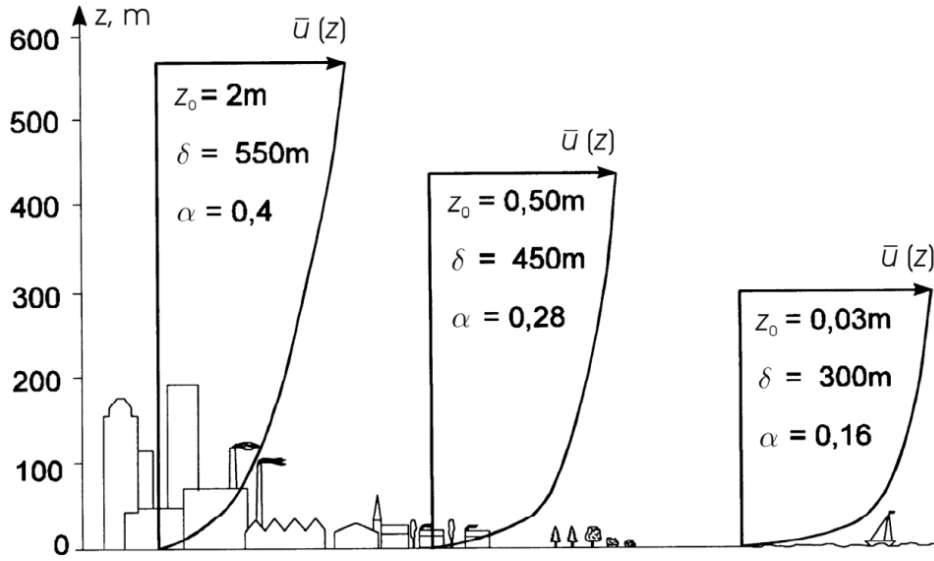
Figure 2.9: Power-law exponent for urban, suburban and rural terrain [17]

While the logaritmic law may be adopted to represent the mean velocity profile throughout the surface layer, the power law is valid for the entire ABL:

$$\frac{\overline{u}_z}{\overline{u}_{\mathrm{ref}}} = \left(\frac{z - d}{z_{\mathrm{ref}} - d} \right)^{\alpha} = \left(\frac{\tilde{z}}{\tilde{z}_{\mathrm{ref}}} \right)^{\alpha} \tag{2.6}$$

This power law is empirical, but its validity is proven in many previous study, e.g. Kozmar [18], [19] and [20]. $\overline{u}_{\mathrm{ref}}$ is the reference velocity at the reference height z_{ref}. The reference value for z_{ref} in meteorology is commonly 10 m. α is the exponent of the power law. Representation of α as a function of z_0 is shown in Fig. 2.10.
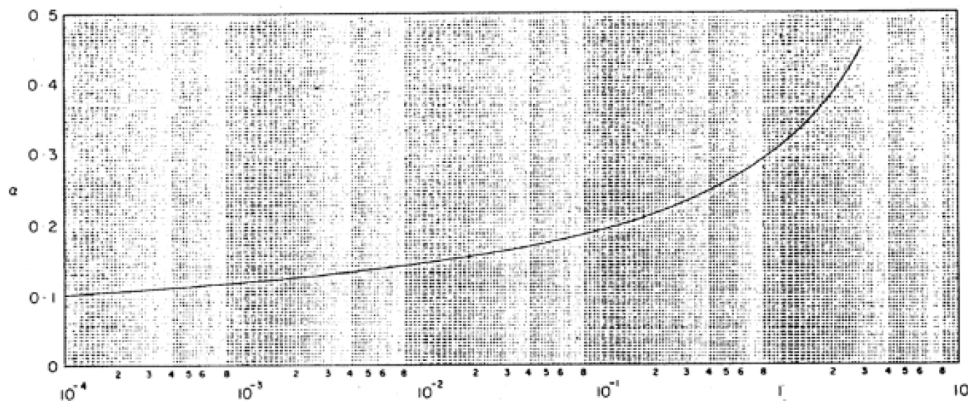
Figure 2.10: Characteristic values of α and z_0 [21]

2.4.   Turbulent wind characteristics

Atmospheric turbulence spans a wide range of length and time scales. Turbulent eddies are important elements in the global circulation, synoptic weather systems, regional circulations, severe storms, clouds, plant canopies and in the ABL. The turbulence in the ABL is a part of a continuous spectrum of atmospheric motions, [22]. The airflow in the ABL is turbulent. Dissipation of the wind kinetic into thermal energy leads to chaotic changes in pressure and velocity of the flow. The turbulence may impact the structures in the following ways, e.g. Kozmar [11]:

- Rigid constructions are exposed to increased unsteady loads due to the wind turbulence;

- Vibrations are emphasized for the flexible structures;

- The structure aerodynamic response is in direct correlation with turbulence characteristics (Fig. 2.11).

Moreover, in addition to the adverse effect on the structural stability, the turbulence may also change pressure distribution on a building, which in turn determines the ACH.
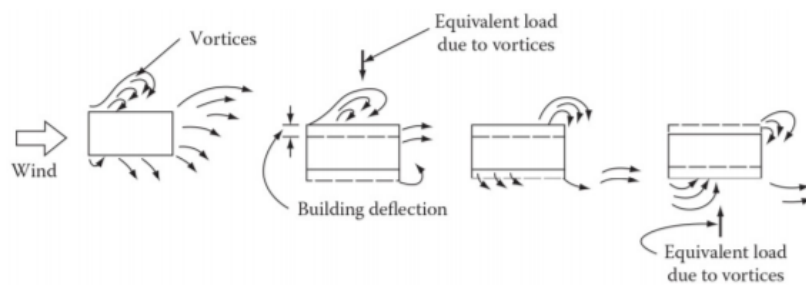
Figure 2.11: Aerodynamic response of a building to the wind [23]

The major relevant parameters that describe the atmospheric turbulence, in addition to the mean flow velocity, are turbulence intensity, integral turbulence length scale, Reynolds shear stress, and power spectral density of velocity fluctuations.

2.4.1. Turbulence intensity

Turbulence intensity in the longitudinal (x), lateral (y) and vertical (z) directions is defined as:

$$I_u(z) = \frac{\sqrt{\overline{u'^2(z)}}}{\overline{u}_{\text{ref}}}, \quad I_v(z) = \frac{\sqrt{\overline{v'^2(z)}}}{\overline{v}_{\text{ref}}}, \quad I_w(z) = \frac{\sqrt{\overline{w'^2(z)}}}{\overline{w}_{\text{ref}}} \tag{2.7}$$

where $u'(z)$, $v'(z)$ and $w'(z)$ are fluctuating components at height z of the absolute velocity u, v and w, respectively. The numerator is the Root-Mean-Square (RMS) of velocity fluctuations, and the denominator is the reference mean velocity commonly determined at the gradient height δ, in the measuring point height or at the studied body height. Measurements in the atmosphere showed that the longitudinal turbulence intensity is larger than the lateral and vertical turbulence intensity and their ratio is nearly constant close to the ground [24]:

$$\frac{I_v}{I_u} = 0.75, \quad \frac{I_w}{I_u} = 0.5. \tag{2.8}$$

Ventilation or air conditioning systems that are perceived to be too ''drafty'' are not that comfortable. It was observed that the ''draftiness'' of air is a function of the turbulence intensity of the moving air [25] and therefore directly related to human comfort in buildings.

2.4.2. Integral turbulence length scale

Turbulent flow can be considered as a family of eddies transferred by the mean flow. Each eddy is characterized by the circular frequency $\omega = 2\pi f$ or by the wave number $k = \frac{2\pi}{\lambda}$, where λ is wavelength and f is frequency. The total kinetic energy of the turbulent flow can be approximated as the sum of the turbulent kinetic energy contained in all eddies. While λ describes the magnitude of a particular eddy, the average size of these energy-containing eddies can be quantified using the integral length scale of turbulence. Each flow direction is characterized by three integral length scales, so for three directions there are in total nine length scales. The most important integral length scale is the one describing the average size of eddies in the longitudinal direction caused by velocity fluctuations in the same direction. Mathematical expression for L_u^x was presented by Sockel [26]:

$$L_u^x = \int_0^\infty R_u^x(\Delta x)\mathrm{d}\Delta x, \tag{2.9}$$

$$R_u^x(\Delta x) = \frac{\overline{u_1'(t) \cdot u_2'(t)}}{\sqrt{\overline{u_1'}^2} \cdot \sqrt{\overline{u_2'}^2}} \tag{2.10}$$

Indices 1 and 2 indicate two different points in space. $R_u^x(\Delta x)$ is the correlation factor. Fig. 2.12 present velocity time history (x-axis is time, y-axis is velocity) in three points of airflow.
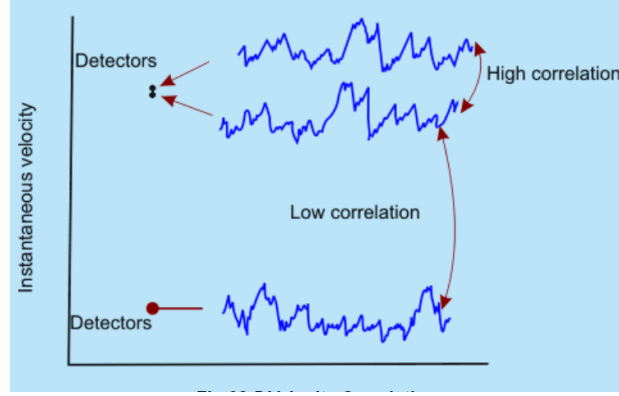
Figure 2.12: Correlation between the points in the airflow [27]

It is obvious that the changes of velocities in time are rather similar in two points characterized by two time records depicted higher in the graph. The third time record lower in the graph differs substantially from two higher time records. With the use of the Taylor's frozen turbulence hypothesis, it is possible to calculate R_u^x as a function of time for each of the time records independently (autocorrelation) as well as by comparing two different time records (cross-correlation).

$$R_u^x(\Delta x) = \frac{\overline{u_1'(t) \cdot u_1'(t - \Delta t)}}{\overline{u_1'}^2} = R_u^x(\Delta t); \tag{2.11}$$

$$L_u^x = \overline{u} \int_0^\infty R_u^x(\Delta t)\mathrm{d}\Delta t. \tag{2.12}$$

2.4.3.   Reynolds shear stress

Laminar flow can be represented as the flow of particles travelling in layers of different velocities. The momentum transfer occurs at the molecular level between the two adjacent particles. On the other hand, the momentum exchange in the turbulent flow occurs at the level of flow particles. The shear stress accordingly develops between the adjacent layers. The molecular momentum transfer leads to the viscous stress $\mu\frac{\partial \overline{u}}{\partial z}$ and the turbulent transfer to the Reynolds shear stress $\rho\overline{u'w'}$:

$$\tau = \mu\frac{\partial \overline{u}}{\partial z} - \rho\overline{u'w'} \tag{2.13}$$

In the atmospheric flows, the viscous stress is at maximum close to the ground. Its influence dramatically decreases with increasing the height from the ground surface. In the inertial sublayer, the Reynolds stress is dominant and the viscous stress can be neglected. Turbulent stress is equal to zero at the surface and strongly increases with increasing the height up to the inertial sublayer where it becomes nearly constant and remains so up to the upper boundary of the inertial sublayer. In the outer layer, its magnitude decreases down to zero at the top of the ABL. In equation (2.13), the Reynolds stress terms $\overline{u'v'}$ and $\overline{v'w'}$ are not considered because they are much smaller than the component $\overline{u'w'}$ and thus neglected.

2.4.4.   Power spectral density of velocity fluctuations

Turbulent flow contains eddies of various sizes with each of them characterized by their turbulence kinetic energy. The power spectral density of velocity fluctuations represents a distribution of the turbulence kinetic energy over frequencies. In wind engineering applications, the most common studied spectrum of the turbulence kinetic energy is the one of velocity fluctuations in the x-direction:

$$\sigma_u^2 = \int_0^\infty S_u(f)\mathrm{d}f, \tag{2.14}$$

where $\sigma_u = \sqrt{\overline{u'^2}}$ is the standard deviation of absolute velocity in the longitudinal direction, $S_u(f)$ is the power spectral density of velocity fluctuations in the longitudinal direction. Large, energy-containing eddies resolve into smaller ones. This leads to the

energy transfer from larger to smaller vortices until the smallest ones dissipate into the heat. This process is called the energy cascade [11] and it is shown by Garratt [28] in Fig. 2.13.
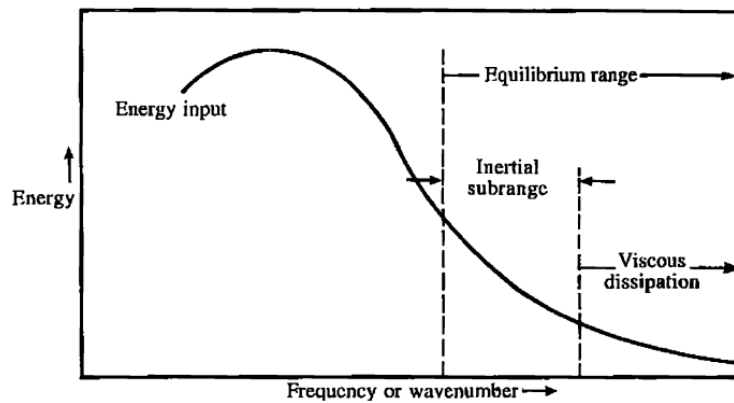
Figure 2.13: Power spectral density of longitudinal velocity fluctuations

The Kolmogorov theory describes how the turbulence kinetic energy is transferred throughout the inertial subrange: $S_u(f) \approx k_w^{-5/3}$, where k_w is the wave number of the eddy. A wide range (meteorological) power spectral density of longitudinal velocity fluctuations is shown in Fig. 2.14.
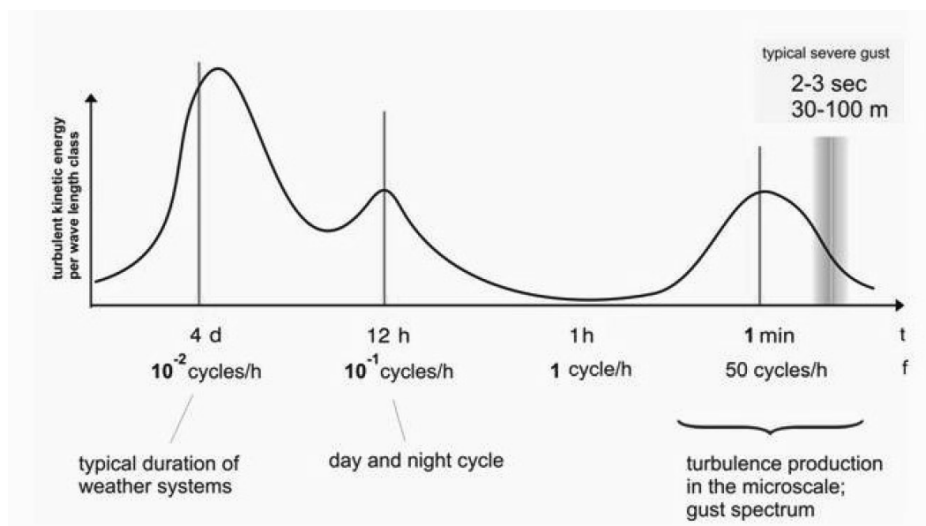
Figure 2.14: Spectral distribution of the turbulence kinetic energy in the atmospheric boundary layer, [29]

Three main peaks are marked and the reason of their existence, lifetime and frequency is noted. In the wind engineering, only the power spectrum with the energy clustered around the peak around 1 min (also reported in Fig. 2.13) is relevant and studied in detail, whereas the energy concentrated around two other peaks (4 days and 12 hours) are more relevant in geophysics, meteorology and climatology.

2.5.   Flow around the cube

Flow and heat transfer in a channel with wall-mounted cubes represent a commonly studied engineering configuration that is relevant in many applications. This simple geometry creates complex vortical structures and generic flow phenomena associated with turbulent flow. Flow patterns around bluff bodies were investigated in detail over the past few decades. Martinuzzi and Tropea [30] and Hussein and Martinuzzi [31] presented their experimental results where they characterized the approaching flow as four main features. There is a standing vortex upstream of the windward facade. Corner streams and flow separation areas develop at the surfaces parallel to the main flow and on the top building surface. An area with a high-velocity gradient is the shear layer. The horseshoe vortex is clearly exhibited.
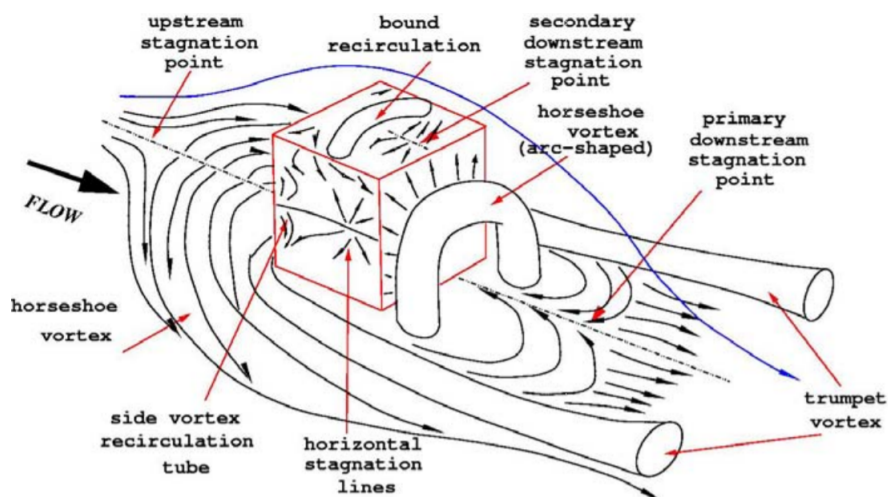
Figure 2.15: 3D representation of the flow around a surface mounted cube, [31]

The wind flow around the building influences pressure distribution on the building facade that in turn impacts the ACH. Surface pressure distribution is commonly provided using

the pressure coefficient:

$$C_p = \frac{p - p_\infty}{\frac{1}{2}\rho V_\infty^2},$$ (2.15)

where:

- p is the total pressure in the measuring point,

- p_∞ is the static pressure in the undisturbed freestream flow,

- ρ is the air density,

- V_∞ is the mean velocity in the undisturbed freestream flow.

A characteristic C_p distribution on a bluff body is shown in 2.16.
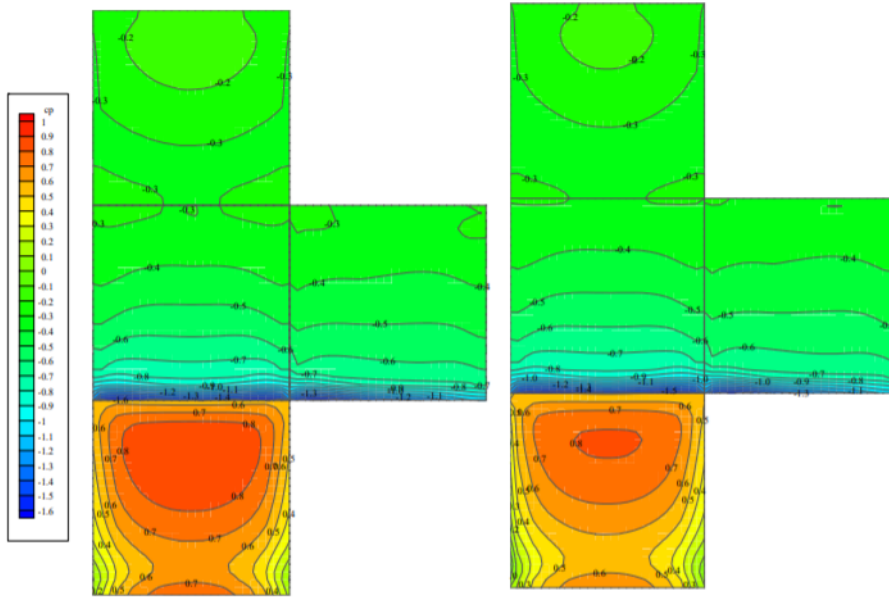
Figure 2.16: Pressure distribution on a body of a cubic shape, results for rural (left), and suburban (right) terrain type [32]

The turbulent flow around the wall-mounted bluff body separates from the leading edges of the body and then eventually reattaches on the top and side surfaces. Positive pressure appears only on the windward surface where the kinetic energy of the flow for the most part converts into pressure. The maximal positive pressure is in the stagnation point. That point is at approximately 70% of the building height. The largest negative pressures occur immediately downstream of the separation lines and are followed by a

substantial pressure recovery on the top and side surfaces. Larger upstream turbulence leads to earlier reattachment and pressure recovery, [33].

Velocity field around neighbouring cubes is presented in Fig. 2.17. These phenomena are particularly important for the ACH of the studied building, which is predominantely influenced by the surface pressure at the outside building surface (facade).
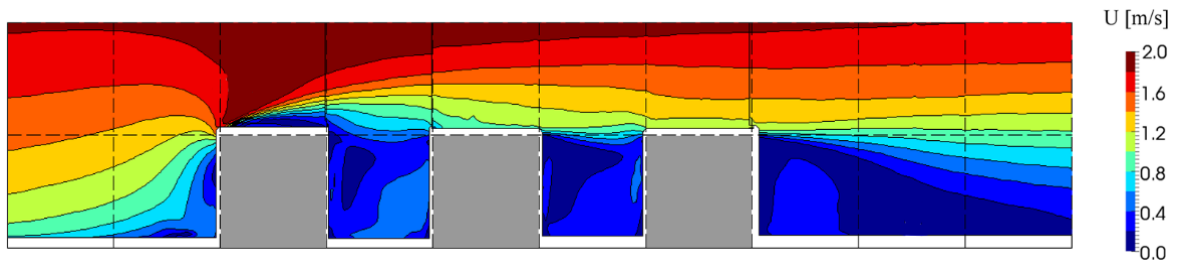
Figure 2.17: Velocity field around neighbouring cubes, side view [34]

Flow impingement and separation on front buildings have a significant impact on downstream buildings. There are standing vortices and other complex phenomena in the gaps between the buildings, Figure 2.18, with more details provided in King at al. [35] and Castro at al. [36].
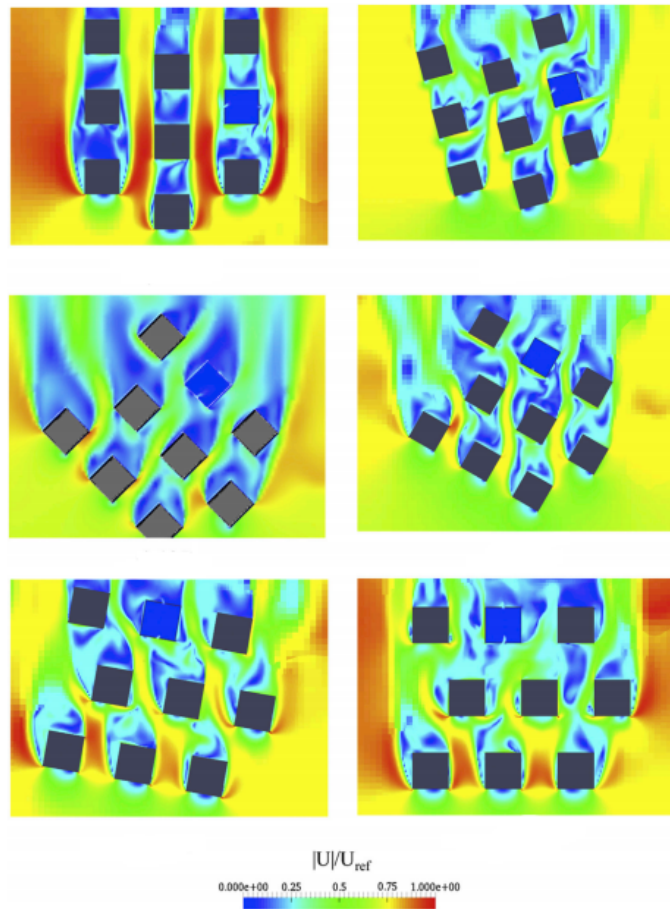
Figure 2.18: Velocity field around neighbouring cubes, ground plan [35]

3 | Experimental setup and measurement methods

There are generally four working approaches in the field of wind engineering and environmental aerodynamics:

- Wind-tunnel experiment;

- Full-scale experiment;

- Computational Fluid Dynamics (CFD);

- Semi-empirical methods.

Semi-empirical methods and CFD, whose development is rapid, are less expensive options. Their results however must be validated by the experiments due to their insufficient accuracy. For the present thesis, the experimental approach was selected and the wind-tunnel experiments were conducted at the Institute of Fluid Mechanics and Heat Transfer at the Graz University of Technology (TUG), Austria.

3.1. Wind-tunnel design

Wind tunnels are generally tube-shaped facilities that allow scientists and engineers to test the aerodynamics of structural models. Air flow in the wind tunnel can represent wind if the model is static in reality, but can also simulate moving object like a car or an aeroplane moving through the still air. As the aim of the present study is to evaluate the intensity of natural ventilation depending on wind characteristics, it is necessary to use the wind tunnel that can simulate various wind characteristics (Fig. 3.1). The IFMHT

in Graz is equipped with two wind-tunnels, i.e. the low-speed aerodynamic wind tunnel and the boundary layer wind tunnel. The latter one is appropriate for this thesis as it can simulate different terrains and their corresponding wind characteristics.

Figure 3.1: Boundary layer wind tunnel at the IFMHT

It is a Göttingen closed-circuit type wind tunnel with the closed test section. The ceiling is adjustable in height so a development of the ABL simulation is not affected by the static pressure gradient along the test section. The total length of the test section is 8.6 m, and 2 m wide and 1 m high at the turntable. The air is circulated with two powerful axial fans. The maximum flow velocity is 40 m/s. The turntable is mounted at the end of the test section. Structural models are commonly placed at the turntable, where it is possible to investigate the effects of various flow incidence angles by rotating

the turntable. For an appropriate thickness of the ABL simulation, the test section should be long because the boundary layer develops rather slowly. To enhance the ABL simulation development, a grid of cylindrical rods was added at the test section inlet. Downstream of the rods there was a sawtooth barrier. The purpose of the barrier is to enhance an equilibrium boundary layer flow in a shortened distance. It is important that the ratio between the boundary layer thickness and the characteristic building dimensions is equal in model and prototype - Jensen similarity. This study aims to evaluate natural ventilation in the suburban and rural environments. The power-law exponent α in the suburban environment was taken as $\alpha = 0.22$ and for the rural terrain $\alpha = 0.15$. The experimental setup in the test section is shown in Fig. 3.2.
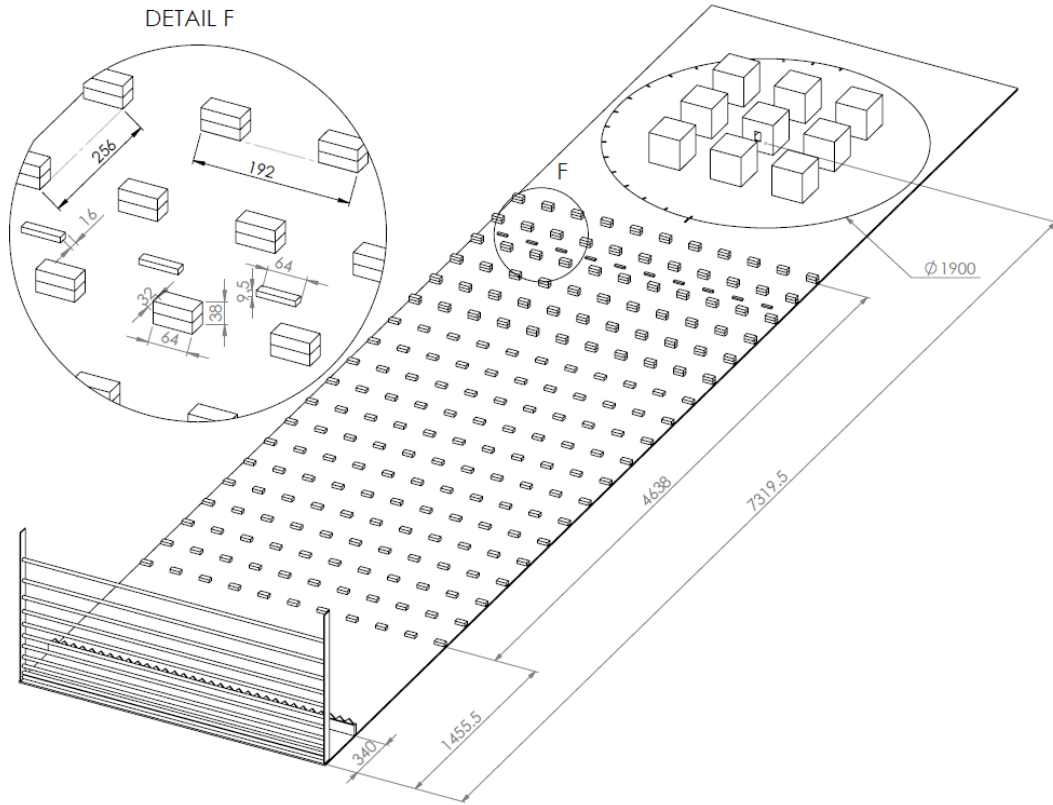
Figure 3.2: Plan view of the IFMHT-GUT wind tunnel with dimensions in mm

For the suburban terrain, surface roughness elements (Lego and Lego Duplo bricks) of different sizes were placed on the test section floor (also on Fig. 3.2). The layout of

bricks was adopted from Langensteiner [1]. There are six rows with two connected Duplo bricks followed by thirteen single Duplo rows. Each row has eleven equally spaced bricks. Between the second and the third row ten basic Lego bricks were added at positions where air would otherwise pass unhindered. The spacing between horizontal rods varies and is shown in Fig. 3.3 The sawtooth edge barrier was 200 mm high in total.

For the rural terrain type, some changes had to be made to satisfy the necessary power law and turbulence characteristics. A suitable configuration was determined by trial and error. The surface roughness was removed and height of the sawtooth edge barrier was decreased by removing its central part. The barrier dimensions are shown in Fig. 3.4 for both types of terrain. Elements and their size are represented in Fig. 3.5, case a) for suburban and case b) for rural terrain.
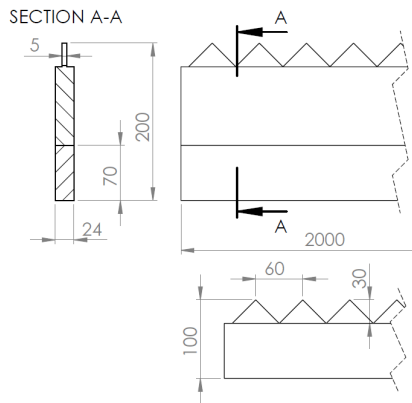
Figure 3.4: Schematic view of the sawtooth edge barrier for suburban (upper) and rural (lower) terrain, dimensions in mm
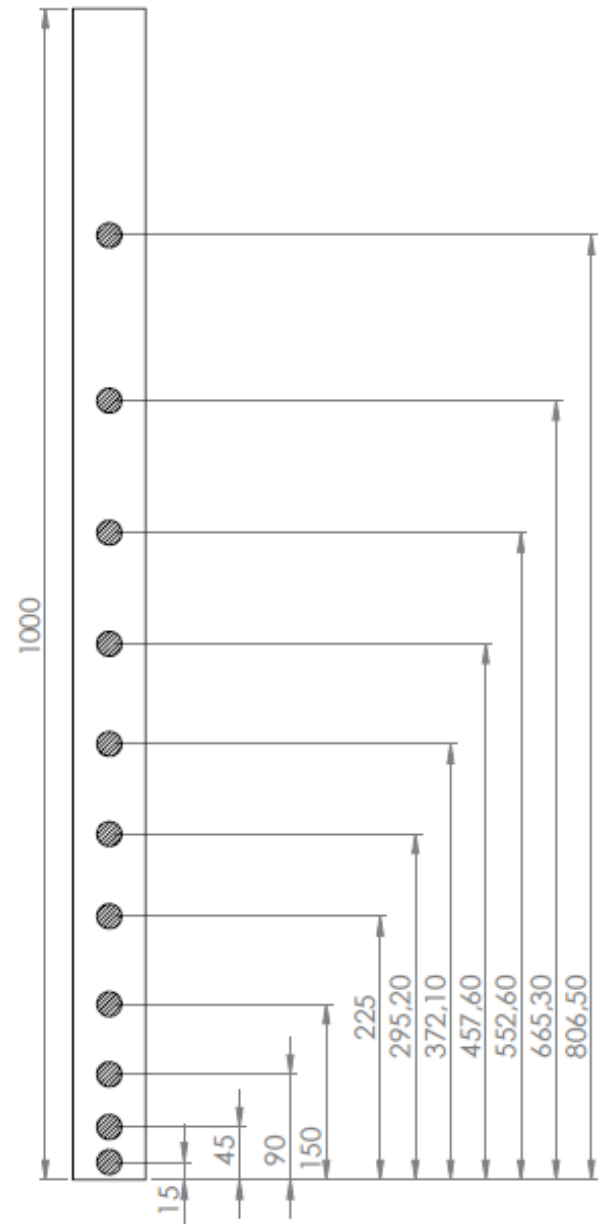
Figure 3.3: Schematic view of the grid of rods, dimensions in mm
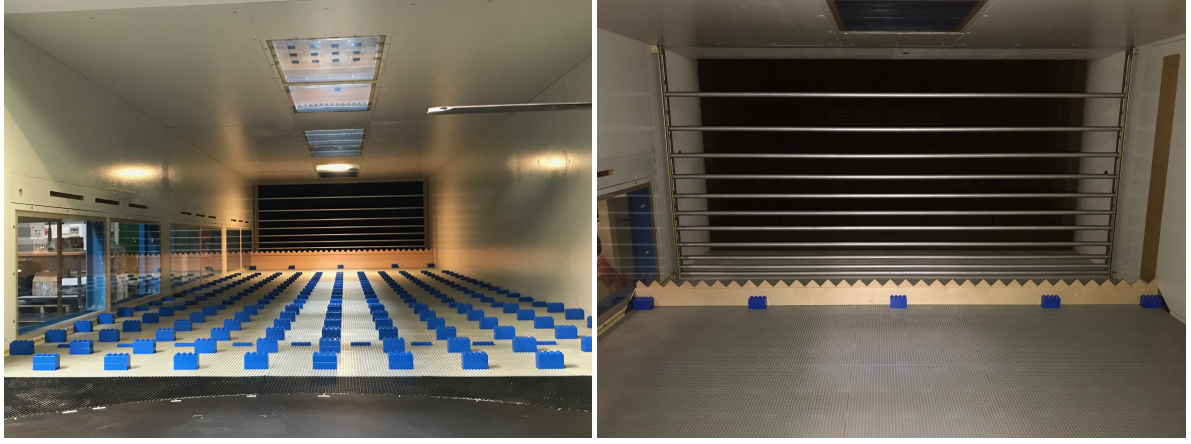
<center>a)   b)</center>

Figure 3.5: Wind-tunnel test section for suburban, a) and rural, b) terrain

During the simulation of natural conditions, it is important that there are no changes in the streamline patterns due to implemented models. These changes may cause different pressure distribution on building model walls. To satisfy this condition blockage of the wind tunnel needs to be as small as possible. In this study the blockage was :

$$\varphi_o = \frac{A_m}{A_n} = \frac{\sqrt{200^2 + 200^2} \cdot 200 \cdot 3}{1000 \cdot 2000} \cdot 100 = 8.49\% \tag{3.1}$$

where A_m is the projection surface of the model and A_n the cross-sectional area of the wind tunnel test section.

3.2.   Building models

The natural ventilation of a cubic building model was studied in arrangements with one and two windows. Dependence of the ACH on the flow incidence angle for both terrain types was determined using the same building model for the single-side and cross ventilation. The building model was previously studied in Golubić [37] as well, (Fig. 3.6 a).
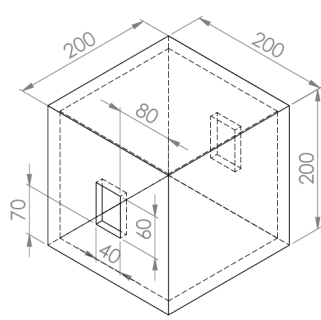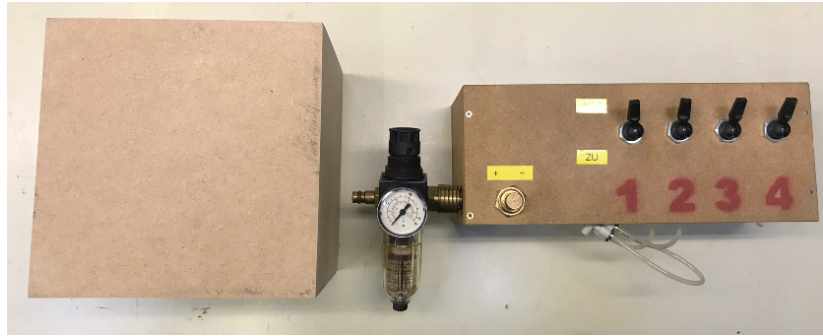
a)   b)

Figure 3.6: Schematic view of the cubic building model a) and control box for pneu-
matically driven sliders b)

The building model is equipped with pneumatic sliders connected to the compressed
air system. Opening and closing of windows is regulated manually using the control
box by releasing or stopping the compressed air, Fig. 3.6 b. Figure 3.7 shows the cube
interior. The roof is removed so that the sliders, pipes for the pneumatics (blue) and
tracer gas (transparent) can be seen.
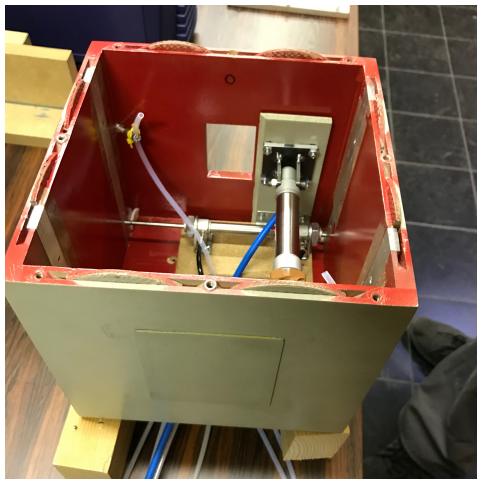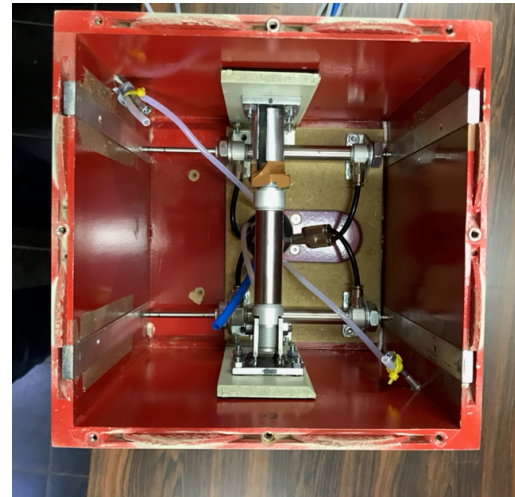
a)   b)

Figure 3.7: Interior of the cubic building model a) with an open window, b) with closed
windows

Walls are made of wood and coated with the special enamel from the inside to suppress
leaking of the tracer gas outside of the cube. For the ACH testing in urban environment,
eight dummy building models were set around the main building in a 3 x 3 pattern.

Dummies are cubes of the same size as the main building model, but without the windows.

3.3.   Experimental arrangements

In order to gain a perspective on the influence of various parameters on building natural ventilation, it was necessary to carry out many experiments with different system configurations. First measurements were carried out for the suburban type terrain. A stand-alone building model was placed in the test section. The ACH was measured for a single-side (1 window open) as well as cross ventilation (2 windows open). The effects of different velocities (3, 5 and 7 m/s) and flow incidence angles were investigated. In the subsequent tests, dummy models were added to simulate the urban neighbourhood. Eight of them were properly arranged around the studied building model. In addition to the flow velocity and its incidence angle, the spacing density between the building models was varied as well. The procedure was repeated for the rural area.

The studied spacing densities of building models:

a)   Small spacing density of building models, i.e. distance between building models $d = 100$ mm or $d = 0.5a$, where a is the length of an edge of the cubic building model ($a = 200$ mm),

b)   Medium spacing density of building models, i.e. $d = 200$ mm$= a$,

c)   Large spacing density of building models, i.e. $d = 300$ mm$= 1.5a$.

Figure 3.8 presents studied model configurations for a stand-alone building model with a single window opened (single-side ventilation).
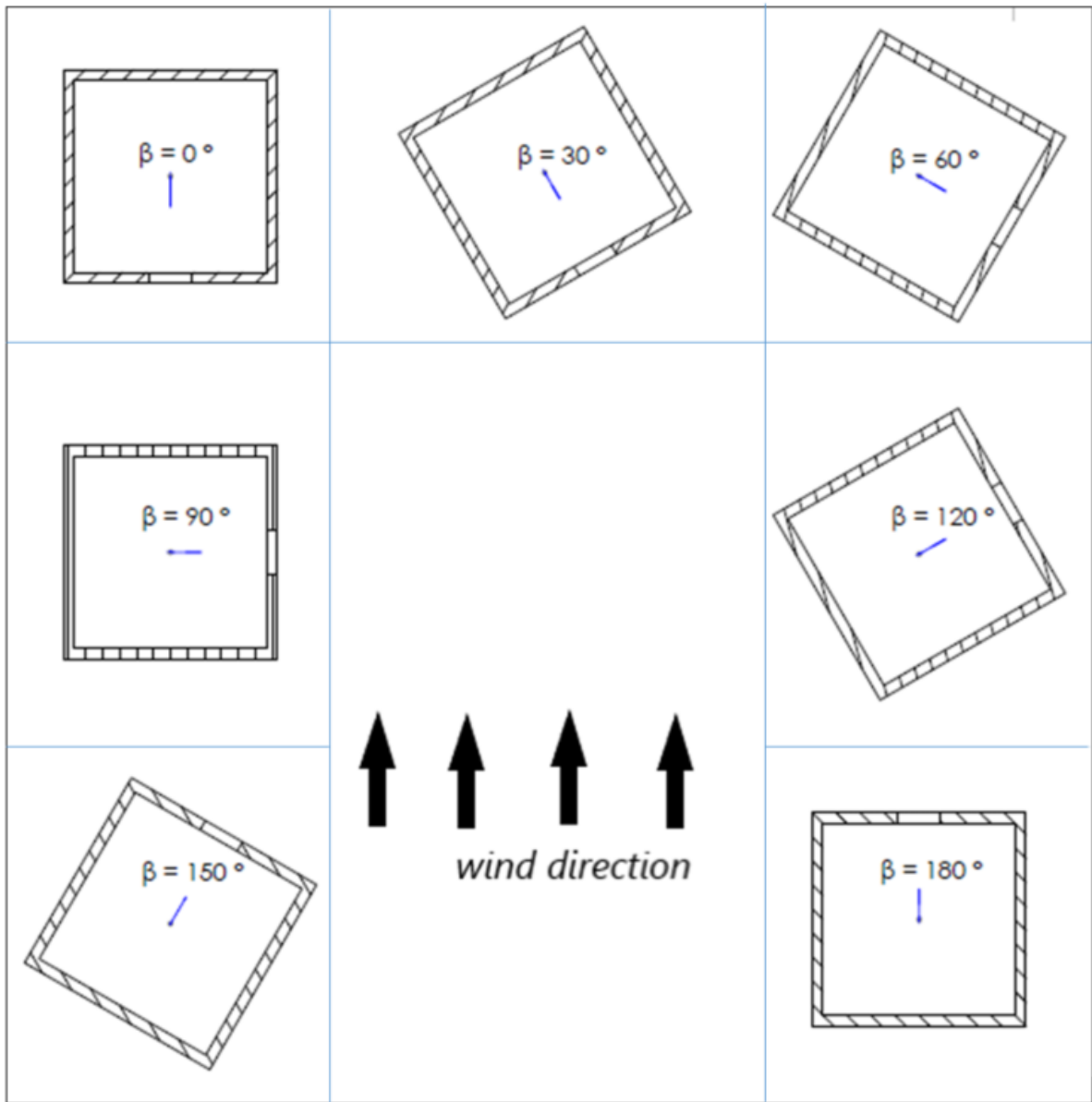
Figure 3.8: Studied configurations for single-side ventilation measurements
on a stand-alone cubic building model

Stand alone building model with both windows open is shown in Figure 3.9 (cross ventilation).
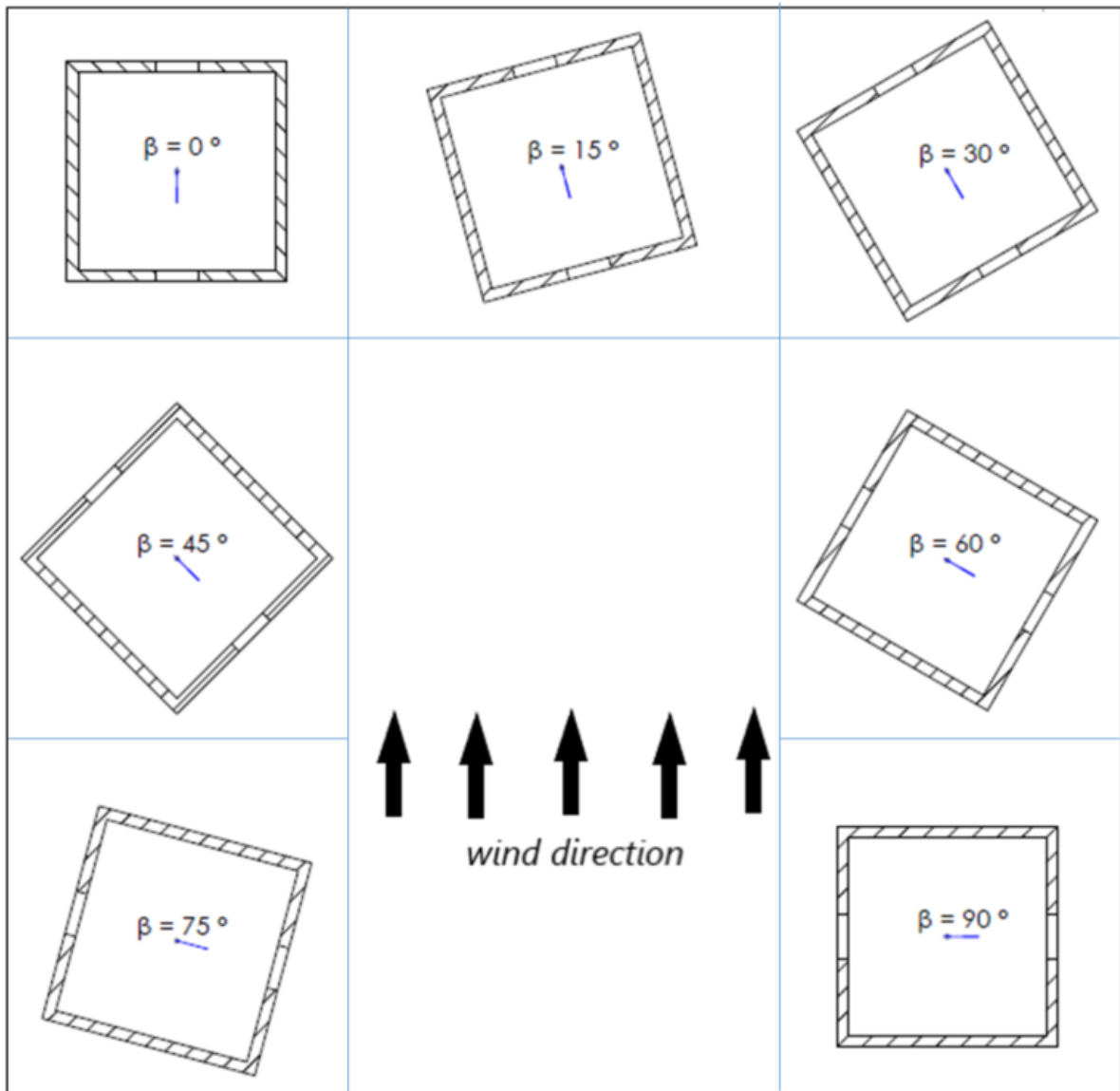
Figure 3.9: Studied configurations for cross ventilation measurements on a
stand-alone cubic building model

A photograph of a 3 x 3 square pattern representing an urban neighbourhood with
different spacing densities among building models is shown in Figure 3.10. The schematic
view of the configurations for cross ventilation and single-side ventilation are shown in
Figures 3.11 and 3.12, respectively.
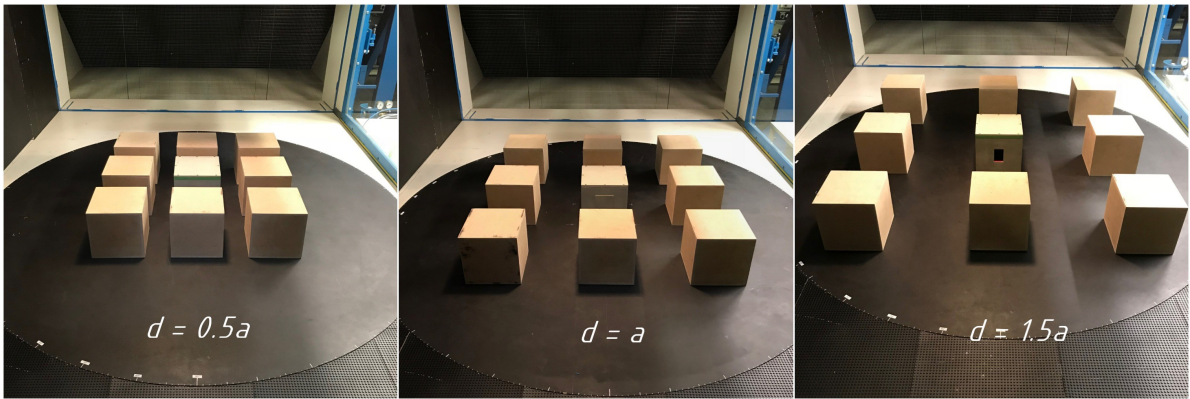
Figure 3.10: Different spacing densities for a 3x3 square pattern of building models
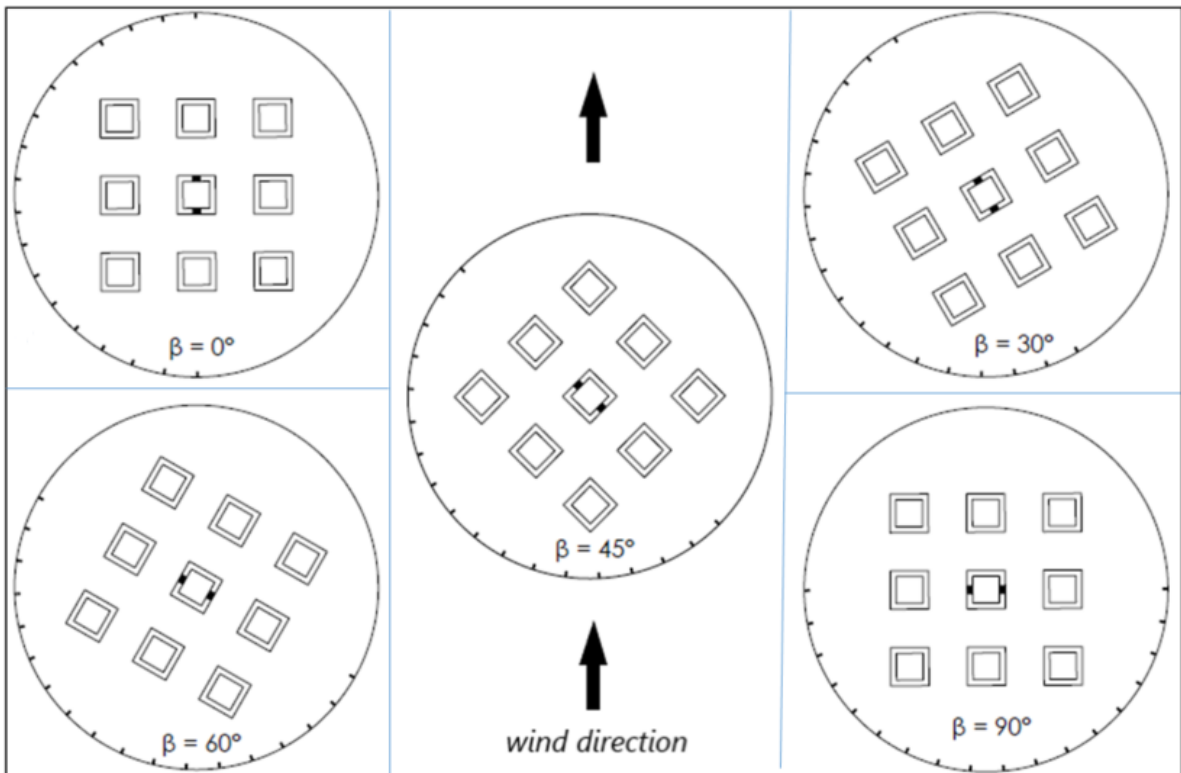
Figure 3.11: Studied configurations for cross ventilation measurements of a building model situated in a neighbourhood model

It should be noted that Figure 3.11 shows configurations for measurements in a rural area. For the suburban area, the flow incidence angles of $0°, 30°, 60°$ and $90°$ were tested.
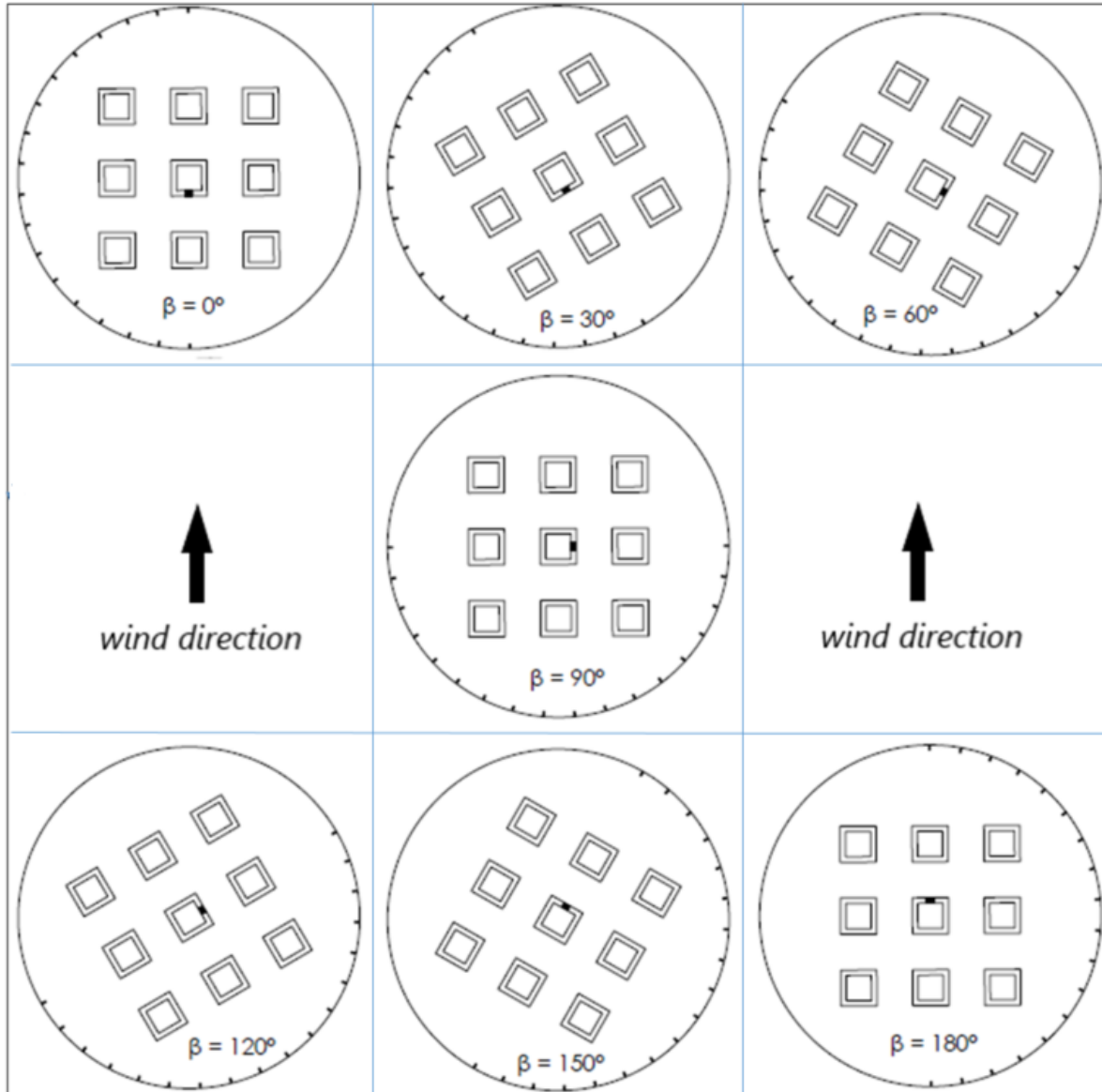
Figure 3.12: Studied configurations for single-side ventilation measurements of a building model situated in a neighbourhood model

3.4.   Velocity measurements

There is a number of requirements that must be satisfied by the velocity measuring apparatus before turbulence can be properly measured, Hinze [38]:

- The detecting element in the flow field must be so small that it causes only minimal disturbance of the flow

- The instantaneous velocity distribution must be uniform in the region occupied by the element. A detecting element must be smaller than the smallest eddy we want to measure. For regular measurements, size of 1 mm should not be exceeded.

- Instrument must have low inertia, so that response to even the most rapid fluctuations is practically instantaneous. For low and moderate flow velocities, frequencies up to 5000 s^{-1} may be expected.

- The sensor must be sufficiently sensitive to record small differences in the fluctuations as they are often only a few percents of the mean velocity.

- Sensor must be stable, sufficiently strong and rigid to exclude vibrations caused by turbulent flow.

A sensor whose development and application for measuring turbulent flow have outstripped those of others is hot-wire anemometer (HWA). Its outstanding characteristics meet all of the parameters listed above, so the HWA was used in the present study as well.

3.4.1.   Operating principle and modes

This method relies on the heat transfer between a small heated sensor connected to an electric circuit and the fluid flow. The sensor is a round wire or a thin film connected between the prongs of a probe. It is made of metal whose electric resistance depend on the temperature. Many kinds of probes and sensors are available. For the present study, Dantec Dynamics 55P61 dual-sensor X wire probe was used, Figure 3.13. X wire means that a probe has two sensors, each measuring one velocity component. Sensors work simultaneously. Probe needs to be placed parallel to the main stream direction

and wires should be exposed to the flow which impinges them at an incidence angle of 45°.
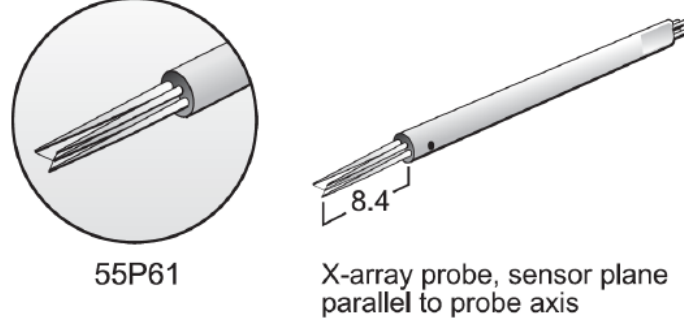
Figure 3.13: Dantec Dynamics 55P61 dual-sensor X wire probe, [39].

As the current is passing through the wire it generates heat (Joule heating). The temperature of wires increases and heat is transferred to the moving air by forced convection. For a turbulent flow the instantaneous heat balance is:

$$m_w c_w = R_w I_w^2 - (T_w - T_a)\phi_{\mathrm{conv}}(u), \qquad (3.2)$$

where the left hand side represents the thermal energy stored in the sensor, and the right hand side is a difference between the heating and cooling the rate. Convection function $\phi_{\mathrm{conv}}(u)$ mainly depends on the fluid velocity. Equation (3.2) reveals that the change in velocity leads to a change in an electric circuit which can be measured. Considering the change in the circuit, three operating modes may be distinguished:

1. Constant Temperature Anemometry (CTA): In this mode a change of velocity u creates a change in current I_w by keeping the R_w constant. With no change in R_w the temperature remains constant.

2. Constant Current Anemometry (CCA): The change of velocity u creates a change in resistance R_w by keeping the I_w constant. R_w is measured.

3. Constant Voltage Anemometry (CVA): The voltage V_w, which is a product of R_w and I_w, is constant and change of the current I_w is measured.

In the present study, velocity was measured using the constant temperature anemometry. Dantec Dynamics multichannel CTA system 54N82 was used, Fig. 3.14.
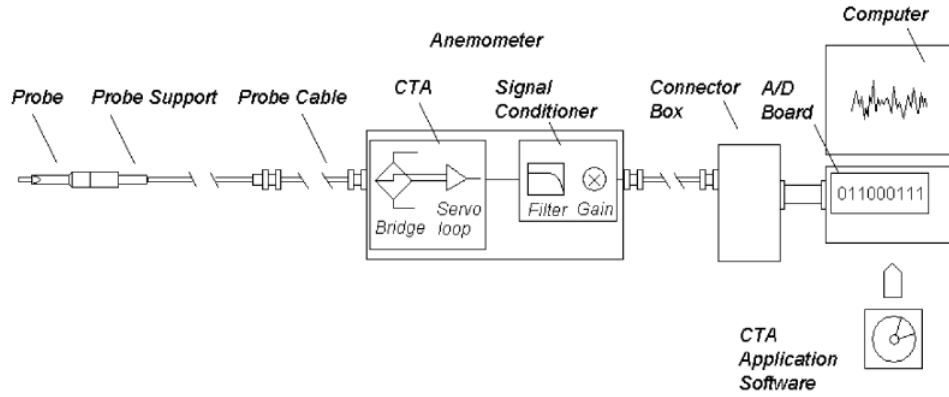
Figure 3.14: Constant Temperature Anemometry (CTA) system [40]

The sensor is fixed on the probe which is mounted on the support. It is connected to the anemometer with the probe cable. Inside the anemometer is the Wheatstone bridge, which has fixed and variable resistors. The regulation maintains constant resistance, and consequently temperature, of the hot wire by adjustment of a variable resistor. Instantaneous changes of temperature are controlled by the servo amplifier, which supplies exactly the same rate of electrical energy to the wire as needed to compensate the convective heat transfer into the environment. Heat transfer is recorded over the voltage of the bridge. From the heat transferred to the air, the velocity of the flow can be calculated. Conditioner for high and low-pass filtering sends a signal to the A/D board. Analog signal is converted into digital so that the analysis can be performed on the personal computer. Dantec Dynamics MiniCTA software was used for the procedures involving the CTA.

3.4.2.   Velocity measurement methodology

Velocity was measured for two main reasons, i.e. a) to determine whether the set configuration properly simulates the characteristics of the examined terrain, b) to control the flow velocity as a parameter for measuring the ACH and to adjust the velocity before starting the traverse movement.

Before simulations of the ABL, the CTA probe with accompanying cables was calibrated in the low-speed aerodynamic wind tunnel. Calibration was performed for velocities in the range from 2 m/s to 16 m/s in 8 different points. Calibration points were fitted using the fourth order polynomial.

In the the boundary layer wind tunnel, the x wire with holders was mounted on the traverse located at the beginning of the test section. Traverse is an automated device for positioning the probe. The traverse movement was vertical to investigate the vertical velocity profiles. Grid for traverse extends to 713 mm and it is divided in 48 points. The points were denser in the lower part because of the larger velocity gradients. Longitudinal and vertical velocity components were measured for each of 48 points. The time record length for each point was 25 seconds at the sampling rate of 10 KHz. Figure 3.15 shows x wire mounted on a support in the measuring position (in front of the turntable).

Figure 3.15: Hot-wire probe mounted on a traverse support in the IFMHT-GUT wind tunnel [37]

Dantec Dynamics reference velocity probe 54T29 (Fig. 3.16) was set at the other side of the measuring section (referring to the traverse), at the height of 500 mm.
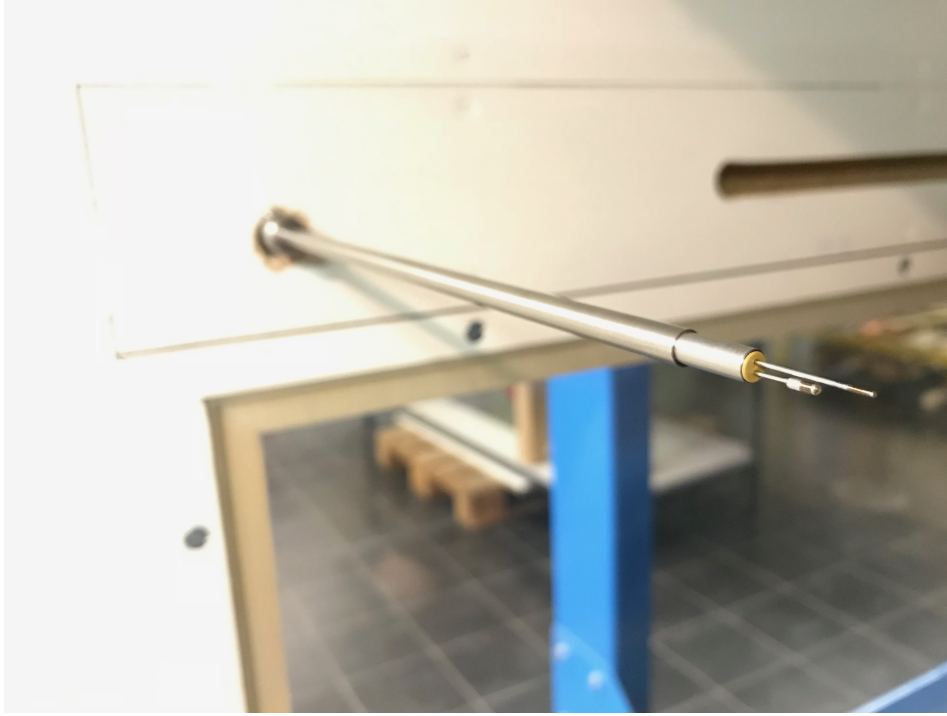
Figure 3.16: Dantec Dynamics reference velocity probe 54T29

ABL simulations were carried out for the suburban and rural type terrains. The ABL characteristics were tested for 3, 5 and 7 m/s. Apart from the lateral centre of the wind-tunnel test section, the ABL simulation characteristics were investigated in plains with 250 mm offset to the right and to the left. That test aimed to verify the uniformity of the flow. The positioning in the lateral direction was done manually.

3.5.   Tracer gas measurements

The main topic of this research, i.e. building natural ventilation, refers to the flow of the outside air in the interior space through various openings on the building. In order to quantify building natural ventilation, the ACH was measured using a tracer gas system. ACH is defined as:

$$\text{ACH} = \frac{\dot{V}}{V_R}. \tag{3.3}$$

V_R is the total volume of the indoor space and $\dot{V}$ is the volume flow rate [1]. There are three versions of this method:

- The concentration-decay method,

- The constant-concentration method,

- The constant-injection method,

whereas in the present work, the concentration-decay method was applied.

3.5.1.   Tracer gas system

For determination of the ACH, infrared (IR) Multi Gas Monitor Innova 1316A-2 of LumaSense Technologies was used. System can work with variety of gases, depending on the needs and conditions of a particular study. In the present study, CO_2 was selected because of its non-aggressive properties. As integral part of the atmosphere, it is neither poisonous nor flammable. In addition to being safe and not harmful to the environment, CO_2 is chemically stable, does not have colour, smell and it does not have taste. Its operating principle is described in the manual [41]:

" The Non Dispersive Infrared Sensors (NDIR) method uses fixed, non-scanning infrared light frequencies to characterize gas concentrations. The concentration of a gas volume is a function of the quantity of gas molecules in the sample. The absorption of IR light increases with the number of gas molecules in the light path. With increase in concentration of infrared-absorbing gas, the transmission of infrared light decreases."

Figure 3.17 shows main elements of the gas analyser.
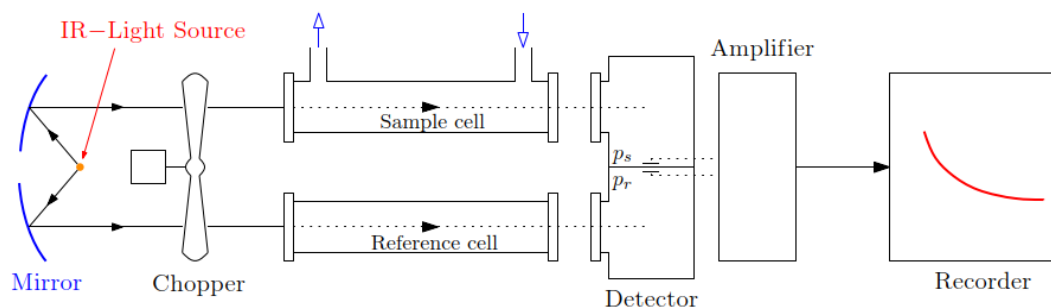
Figure 3.17: Non Dispersive infrared gas analyser, [1]

An infrared light source emits the light of wide frequency range, including IR. One path of the light passes through the reference cell, filled with a non-absorbing gas such as nitrogen. The other path goes to the sample cell. A sample cell is filled with the tracer gas sample that is to be analysed. Gas is pumped into the chamber through the tubes, whose other end is placed in the model (Fig. 3.7). The IR source continuously sends IR waves through the gas tubes. The detector measures the intensity of wavelengths for both paths of the light separately. The intensity of the waves going through the reference cell is not reduced. If the CO_2 gas is present in a sample cell, the detector will read a reduced intensity of appropriate wavelengths. The difference in reading is proportional to the amount of absorbing gas in the sample cell, i.e. CO_2 gas. The signal from the detector is amplified and sent to the computer where it is recorded in the BZ6013-1316A-2 LumaSense program.

3.5.2.   Tracer gas measurement methodology

Concentration decay method implies the initial filling of the internal model space with a tracer gas, while all the openings are closed. After some time, tracer gas and air make a homogeneous mixture. Mixing time depends on a concentration of a tracer gas. The mixture was considered homogeneous when the measured concentration, monitored in the BZ6013 program, ceased to be altered. Then windows were opened using switches on a control box for fixed time interval $\Delta t = t_2 - t_1$. During that time, fresh air was entering and flowing through the indoor space at the previously set velocity. If the model walls are taken as the boundaries of the system, mass conservation law for the tracer gas is:

$$\frac{\mathrm{d}m}{\mathrm{d}t} = C_o \dot{m}_{oi} - C_i \dot{m}_{io} + E, \tag{3.4}$$

where m is the mass of the tracer gas within a model, C is tracer gas mass concentration, $\dot{m}$ is mass flow rate and E is mass injection rate of the tracer gas. Subscripts i refers to indoor and o to outdoor space. The mass of tracer gas is related to the mass of the inside air M by the concentration of the tracer gas in the indoor air C_i:

$$m = C_i M. \tag{3.5}$$

While windows are open, the tracer gas is not injected into the model, so the last member of the Eq.(3.4) is zero. It is assumed that the air mass entering the model is equal to

the mass leaving it $\dot{m} = \dot{m}_{io} = \dot{m}_{oi}$. With these assumptions Eq.(3.4) transforms into:

$$M\frac{\mathrm{d}C_i}{\mathrm{d}t} = \dot{m}(C_i - C_o).$$ (3.6)

With $\Delta C = C_i - C_o$, the mass flow rate is:

$$\dot{m} = \frac{M\dfrac{\mathrm{d}C_i}{\mathrm{d}t}}{\Delta C}.$$ (3.7)

If the mass over volume and density is $\dot{m} = \rho\dot{V}$ and $M = \rho V_R$, where V_R is the volume of the observed space, ρ is the constant air density, and $\dot{V}$ is volume flow rate and after integrating Eq.(3.7) over a defined time period we get:

$$\frac{\dot{V}}{V_R} = \mathrm{ACH} = \frac{1}{\Delta t} \ln \frac{\Delta C(t)}{\Delta C(t + \Delta t)}.$$ (3.8)

The ACH can therefore be calculated from the measurements of the concentration drop in a given time. Concentration was measured before the opening of the windows (after mixing time), and after closing them again. After closing the windows, it was necessary to wait for the mixture to become homogeneous. Concentrations were recorded, and the process was repeated. After collecting enough data to see what values deviate from the average, they were removed and the average value of the others was calculated. A dimensional analysis yields the ratio of the ACH for model and prototype:

$$\frac{\mathrm{ACH}_r}{\mathrm{ACH}_m} = \frac{1}{S}.$$ (3.9)

Where S is the simulation length scale factor calculated in the following section, S determines how many times is the ACH measured in the lab larger than the actual one.

4 | Results

In order to investigate the influence of wind characteristics on building natural ventilation, it was necessary to simulate the ABL flow. The ABLs of interest were those developing above the suburban and rural type terrains. Therefore, the simulation results of the ABLs will be presented first. When the results from the laboratory matched those from the full-scale, the ACH was measured. The obtained data were compared with the available literature. The results for the rural terrain are marked with the triangular shapes and full line, for the suburban terrain with the squares and dashed line.

4.1. Simulation of the atmospheric boundary layer

4.1.1. Mean velocity profiles

Velocity profiles matched well the required conditions for the rural and suburban type terrains. The mean velocity profile was plotted in linear, semi-logarithmic and double-logarithmic scale. A dependence of the mean velocity profile on the height represented by the power law in the double-logarithmic scale reveals a straight regression line. The gradient of that line indicates α, Fig. 4.1.
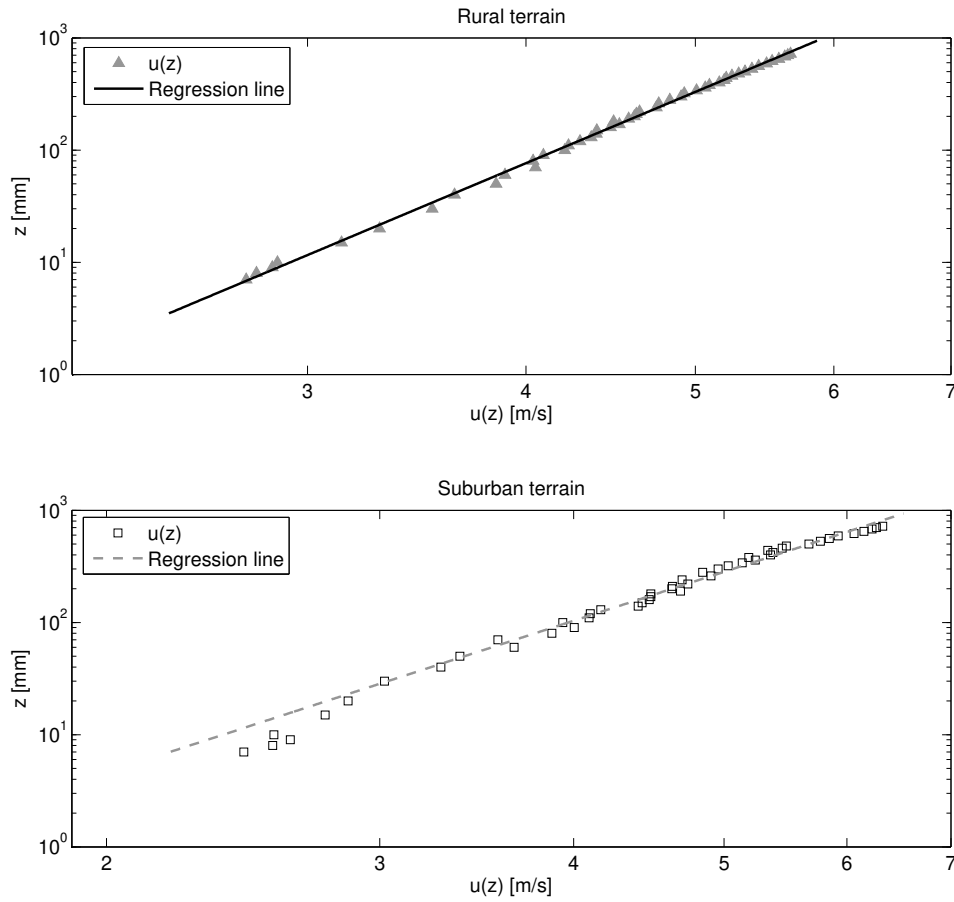
Figure 4.1: Mean velocity profiles for $u = 5$ m/s in a double-logarithmic scale

Values of α calculated from the regression lines are:

Table 4.1: Calculated values of α for the rural and suburban terrain types

α	3 m/s	5 m/s	7 m/s
Rural	0.145	0.152	0.152
Suburban	0.202	0.222	0.229

The mean values of α agree well with the preset values of 0.15 for the rural and 0.22 for the suburban terrain types. Table 4.2 lists the mean velocity parameters of various wind standards. $\alpha = 0.15$ corresponds to the second category (open terrain, island, flat area and water etc.), and 0.22 is between the third and fourth category (suburban, town, small city etc.). These power-law exponents will be used for the comparison with the measured data.

Table 4.2: Description of various terrain types according to several wind standards [42]

category	Exposure (description)	roughness length $z_{0\ (m)}$	Power exponent α	Current code specifications ($z_{0\ (m)}$)
Cat I	Open water (open sea or lake and coastal areas with few obstructions)	0.002	0.103	AIJ Cat I – open sea (0.0014) AS/NZ Cat 1 – open terrain (0.002) BS6399 – Sea (0.003) EN Cat 0 – Open sea (0.003) ISO Cat 1 – open sea (0.003) ASCE Exp D – flat area & water (0.0039) GB Cat A – Sea, island, desert (0.0076)
Cat II	Open country (terrain with scattered obstructions up to 10m high. Rural areas with a few low rise building)	0.04	0.15	EN Cat I – lake & area without obst. (0.01) AS/NZ Cat 2 – open, few small obst. (0.02) NBCC Exp A – Open terrain (0.025) BS6399 – Country (0.03) ISO Cat 2 – open country (0.03) AIJ Cat II – open, few obstruction (0.04) ASCE Exp C – open, few med. obst.(0.048) EN Cat II – area with few obst. (0.05) GB Cat B – village, countryside (0.061)
Cat III	Forest/Sub-urban scattered low(3-5m) buildings (Numerous closely space 3-5m obstructions)	0.2	0.198	AS/NZ Cat 3 – many medium obst. (0.2) AIJ Cat III – suburban (0.21) BS6399 – Town (0.3) EN Cat III – suburban, forest (0.3) ISO Cat 3 – Suburban (0.3)
Cat IV	Urban, large town (many medium height(10-50m) buildings)	0.5	0.241	GB Cat C – City (0.34) ASCE Exp B – Urban (0.58) NBCC Exp B – Suburban & urban (0.58)
Cat V	City, (medium height buildings mixed with tall(50m+) buildings)	1.0	0.289	AIJ Cat IV – City medium height bldg. (0.78) EN Cat IV – Area 15% Bldg >15m (1.0) GB Cat D – City iall bldg (1.13)
Cat VI	City centre (concentration of very tall buildings mixed with other buildings)	>=2.	0.362	AIJ Cat V – City tall bldg. (1.82) NBCC Exp C – City centre (1.97) AS/NZ – city (2.0) ISO Cat 4 Urban (3.0)

Further analysis has revealed the logarithmic law components, i.e. z_0 and u_τ. Data were plotted on a semi-logarithmic scale. The straight regression line was set to fit the experimental data. The intersection point between the y-axis and the regression line presents z_0, and its inclination presents u_τ. Semi-logarithmic plot is shown in Fig. 4.2.
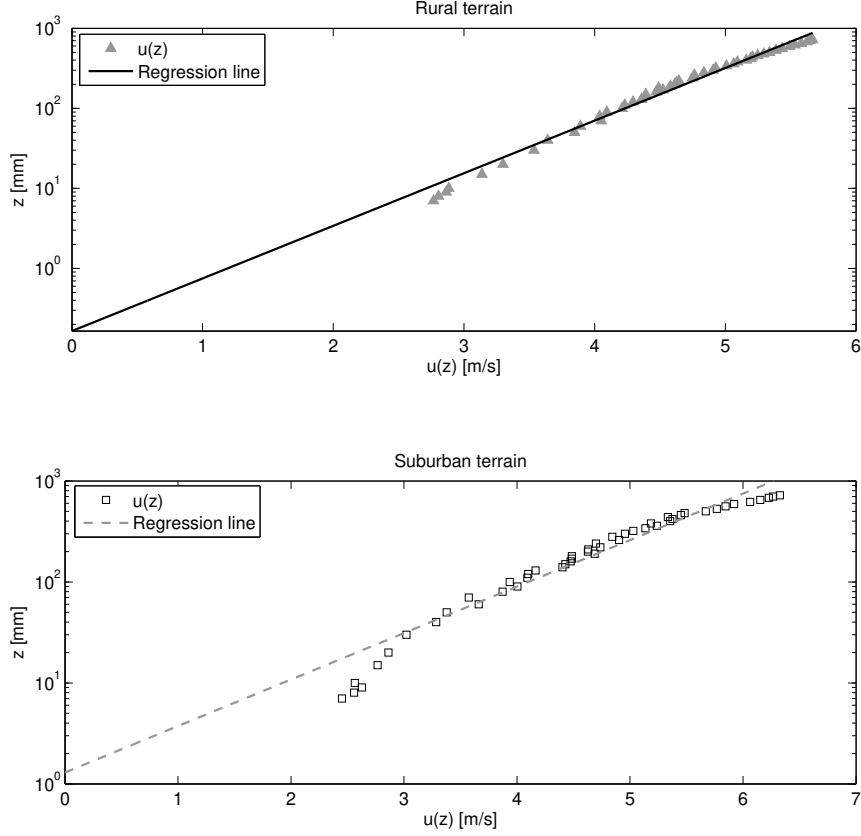
Figure 4.2: Mean velocity profiles for $u = 5$ m/s in a semi-logarithmic scale

The average friction velocities for the rural and suburban terrain types u_τ is 0.271 m/s and 0.387 m/s and the aerodynamic surface roughness lengths $z_{0,m}$ is 0.130 mm and 1.153 mm in the model scale, respectively. The results in Fig. 4.3 indicate the lateral uniformity of the flow. Quantities are reduced to the corresponding values at the height of the reference probe, i.e. 500 mm model scale.
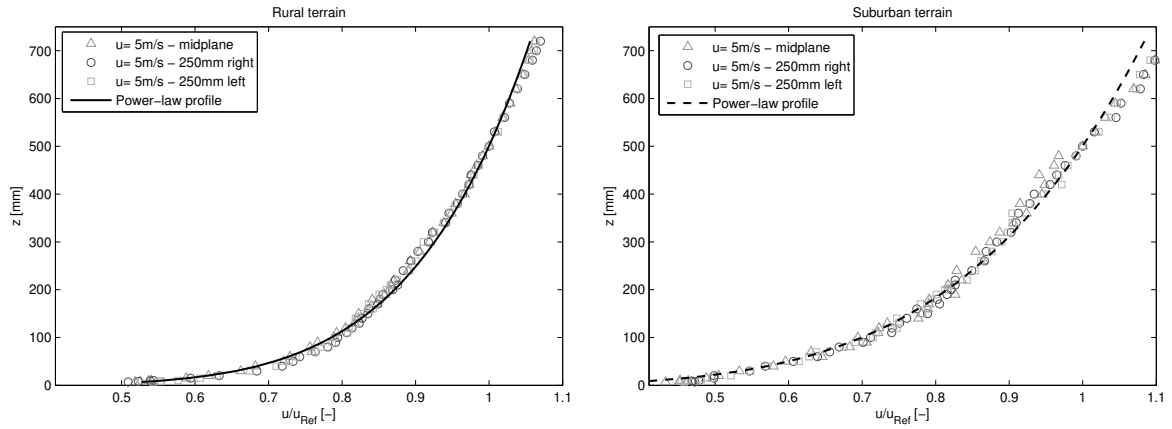
Figure 4.3: Mean velocity profiles for $u = 5$ m/s measured in three different lateral planes for both terrains and their comparison with the power-law profile

The results reported in Fig. 4.4 (normalized using the reference velocity of 5 m/s) indicate successful ABL simulations in comparisons with their respective power-law curves and in Fig. 4.5 with the logarithmic law.
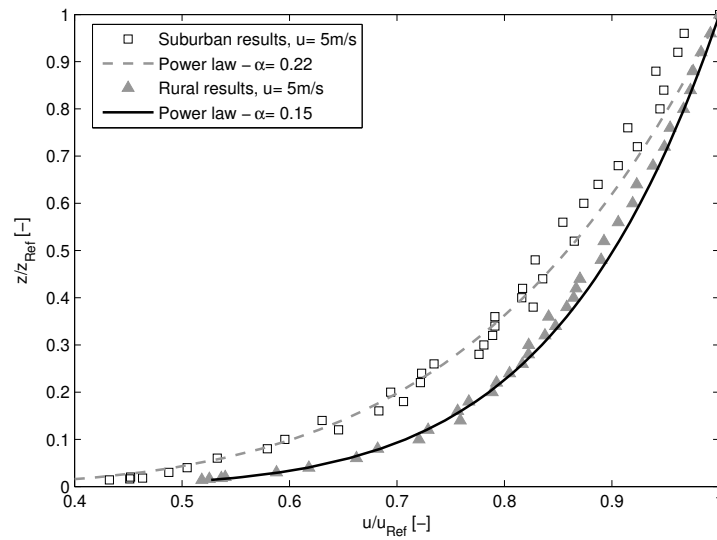
Figure 4.4: Comparison of the rural and suburban mean velocity profiles
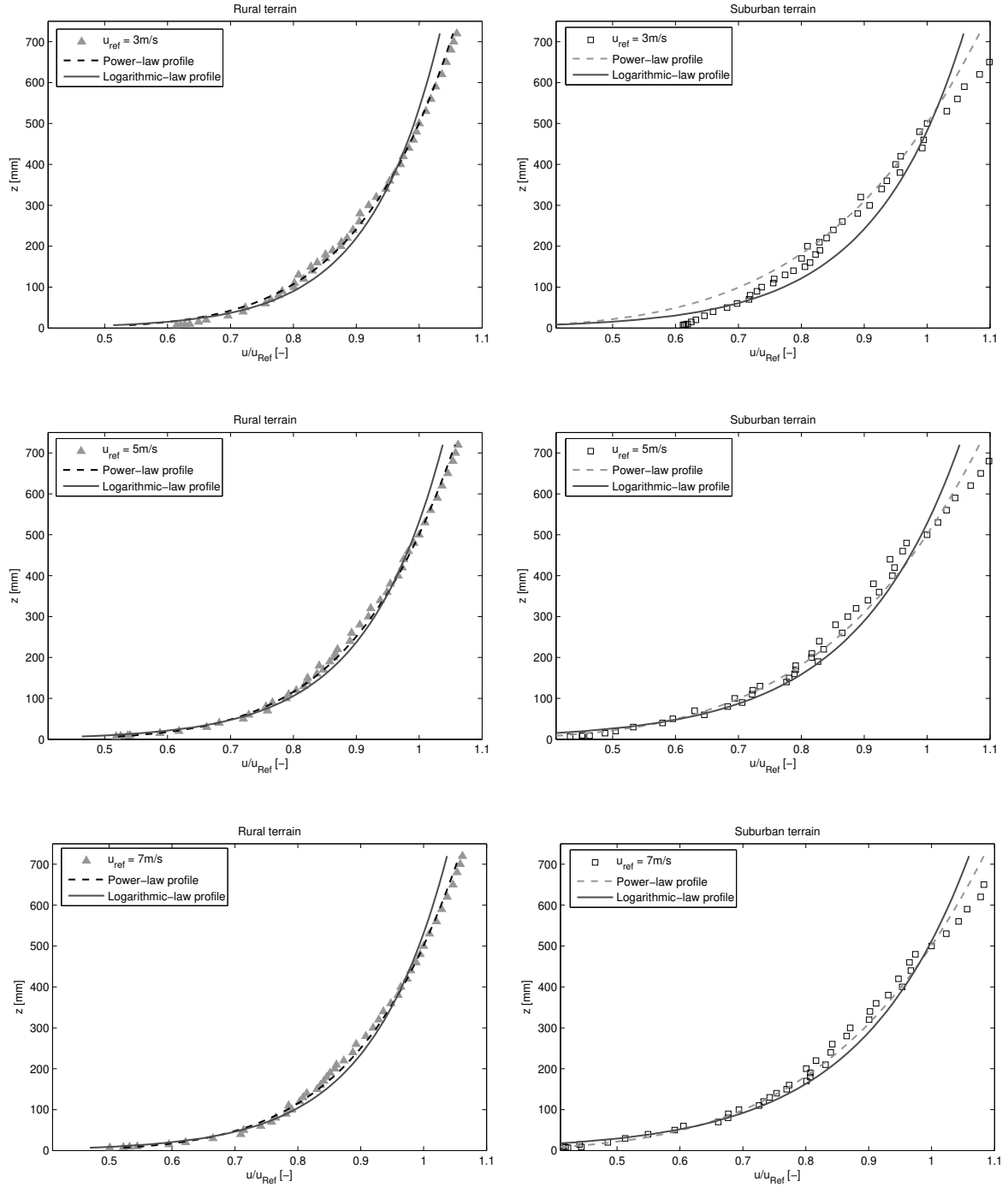
Figure 4.5: Mean velocity profiles compared to the power and logarithmic laws

The rural ABL profile has a larger velocity gradient close to the ground, which is expected for the smoother ground surface.

Simulation length scale factor

The simulation length scale factor was calculated according to Cook [43]:

$$S = \frac{91.3(z - d)^{0.491}}{(z_0)^{0.088} (L_{u,x})^{1.403}}.$$ (4.1)

Scale factors were calculated for each measuring point separately using Eq. (4.1). The average value of all the points is the simulation length scale factor. For both ABL simulations it is 1:250. Scaling-up the model aerodynamic surface roughness length $z_{0,\mathrm{m}}$ yields the prototype aerodynamic surface roughness length $z_{0,\mathrm{p}}$. For the rural terrain type $z_{0,\mathrm{p}} = 0.0325$ m which agrees with the second terrain category ($z_0 = 0.01$-0.06 m) in Table 4.2. This terrain type is described as a rural area with a few low-rise buildings. Measurements for the suburban terrain type yielded $z_{0,\mathrm{p}}$ = 0.288 m. This $z_{0,\mathrm{p}}$ characterizes the third terrain category ($z_0 = 0.2$ - 0.3 m) described as the forest/suburban scattered low (3-5 m high) buildings.

4.1.2.   Turbulence characteristics

Turbulence intensity

The turbulence intensity profiles in the vertical I_w and longitudinal I_u direction are shown in Figs. 4.6 and 4.7, respectively. The results for the longitudinal direction are compared with ESDU 85020 [14] for an appropriate range of $z_{0,\mathrm{p}}$ value for each terrain type.
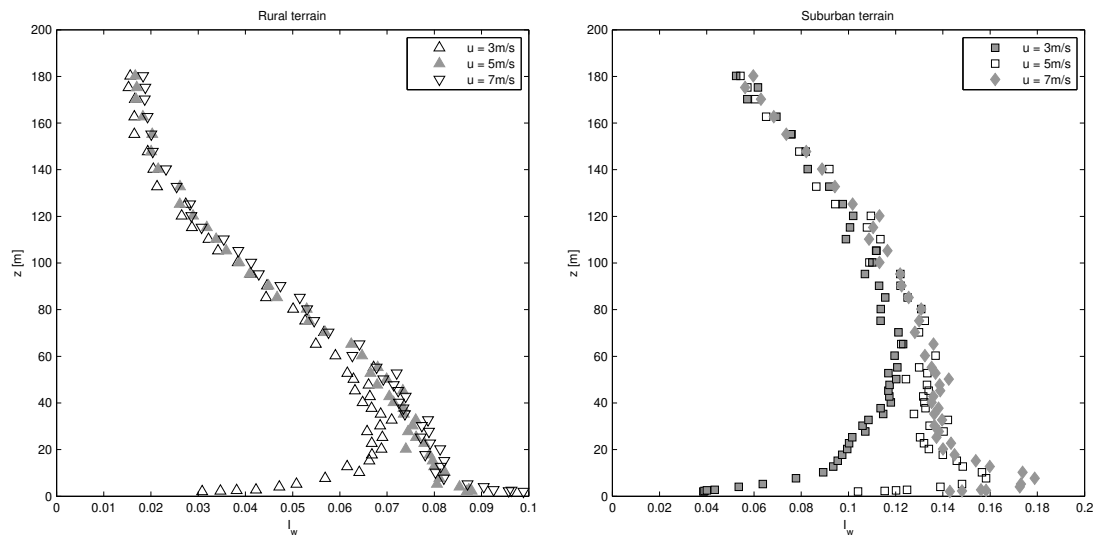
Figure 4.6: Turbulence intensity profile - vertical component I_w
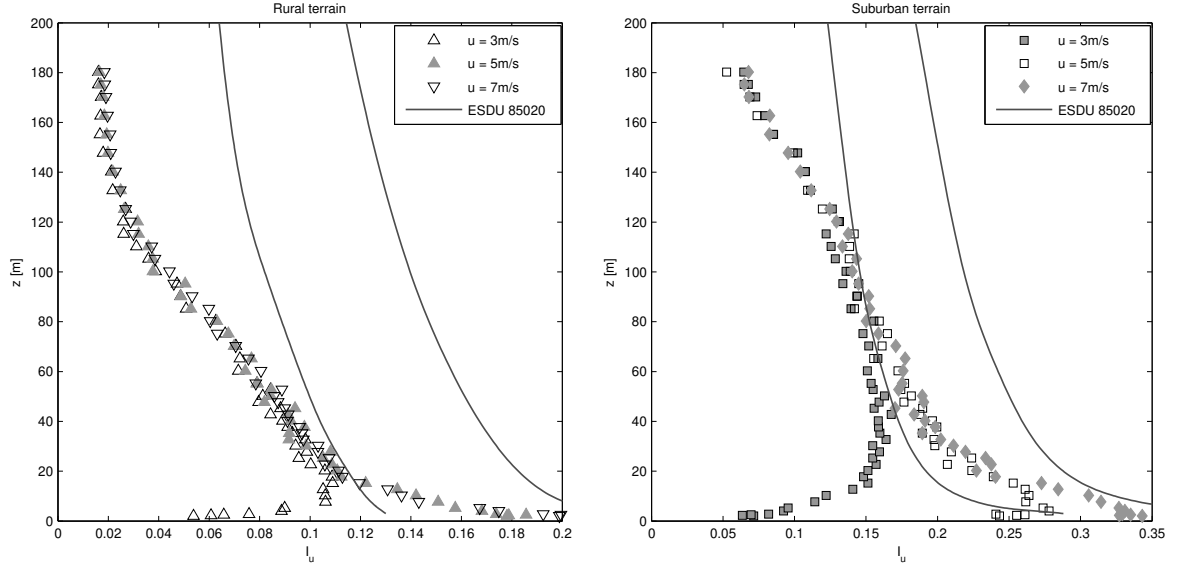
Figure 4.7: Turbulence intensity profile - longitudinal component I_u

ESDU 85020 [14] agrees with the measured values only in the lower ABL region. Curves for 3 m/s do not fall into the recommended area likely due to a small flow velocity, i.e. Reynolds number issues.

Integral turbulence length scales

The obtained integral turbulence length scales are plotted in Fig. 4.8. The results are presented in the full-scale measures.
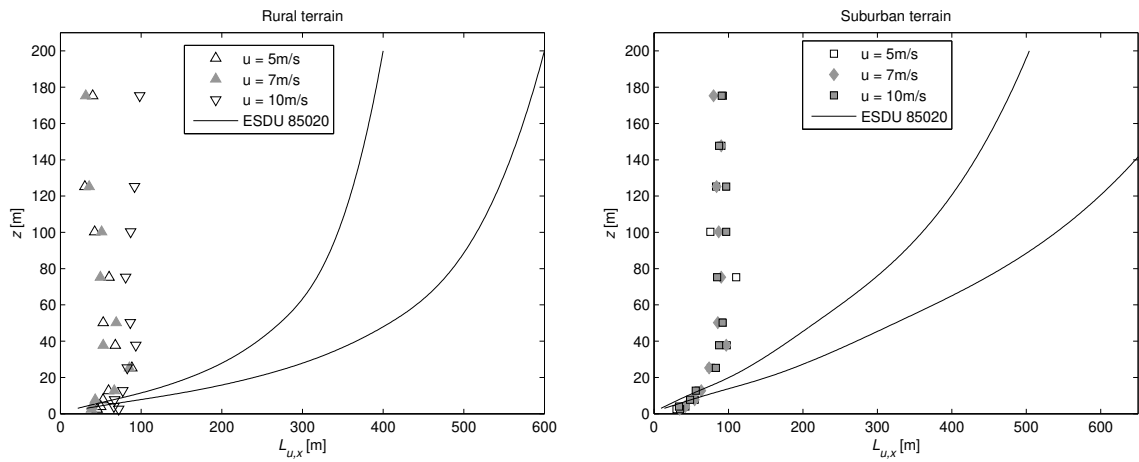
Figure 4.8: Integral turbulence length scales in comparison with the respective ESDU 85020 values

In both ABL simulations, close to the ground, the integral length scales increase with increasing the height and remain constant with further increasing the height. This phenomen was previously observed in other studies as well and it is due to the confined wind-tunnel test section that prevents large eddies to develop.

Reynolds shear stress

The Reynolds shear stress profiles are presented in Fig. 4.9.
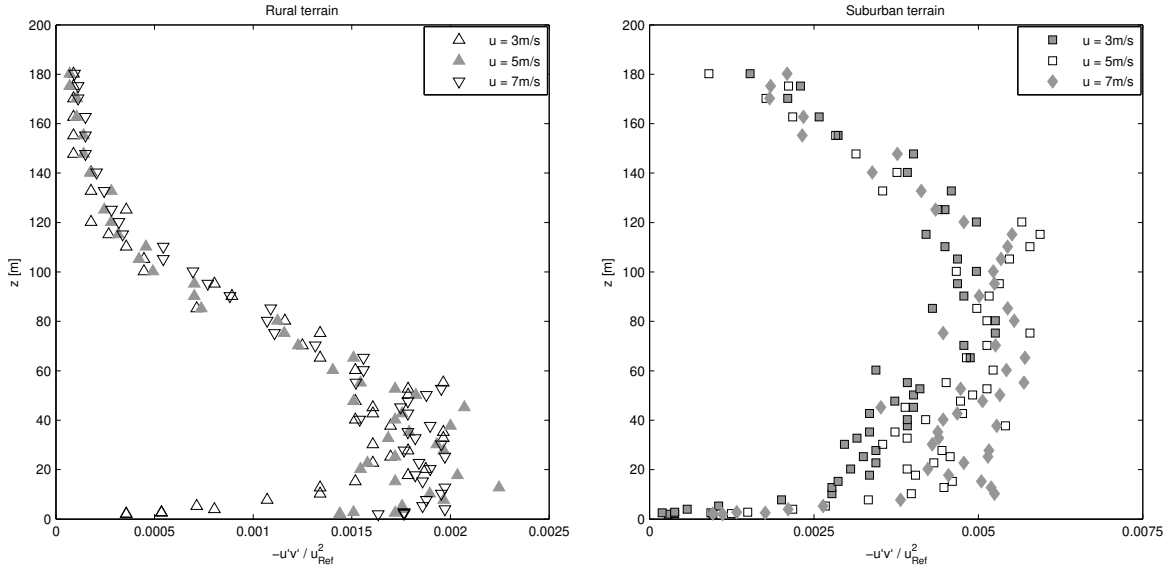
Figure 4.9: Reynolds shear stress profiles

The reference velocity applied to calculate the Reynolds shear stress is the one at the height of the reference probe (500 mm). The Reynolds shear stress is zero at the ground, increases with increasing the height up to the inertial sublayer where it becomes nearly constant. It is clear that the inertial sublayer of the rural ABL simulation is smaller, which is in agreement with the atmospheric physics, as the Prandtl constant-flux layer was observed to be thicker above rougher surfaces.

Power spectral density of velocity fluctuations

The power spectral density of longitudinal velocity fluctuations in Figs. 4.10, 4.11 and 4.12 is in agreement with von Kármán. The inertial sublayer characterised by the constant (Kolmogorov) slope is clearly visible.

Figure 4.10: Power spectral density of longitudinal velocity fluctuations at $z = 10$ m full scale

Figure 4.11: Power spectral density of longitudinal velocity fluctuations at $z = 25$ m full scale
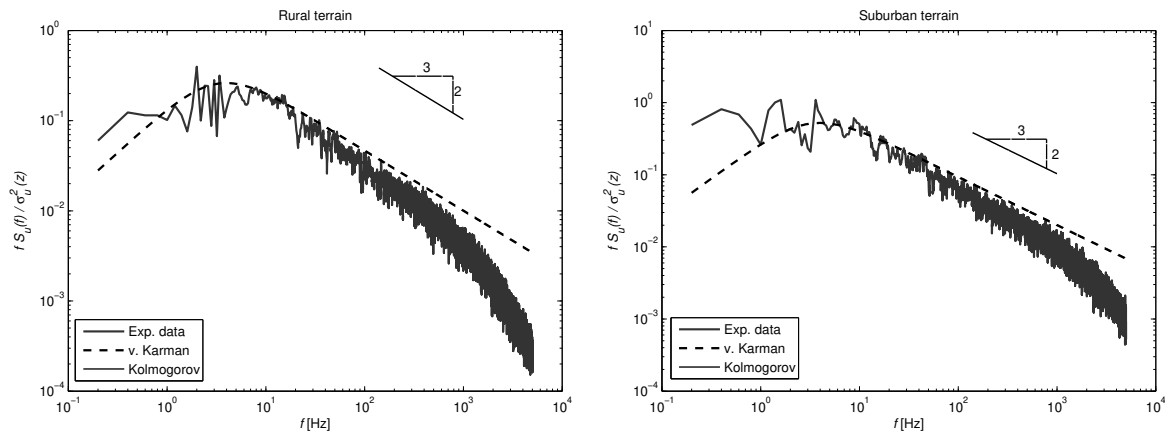
Figure 4.12: Power spectral density of longitudinal velocity fluctuations at $z = 75$ m full scale

4.2.   Building natural ventilation

In this section, the results of the ACH measurements are presented and discussed. The analysis is based on the influence of the terrain type, flow incidence angle β, velocity and spacing density of surrounding buildings.
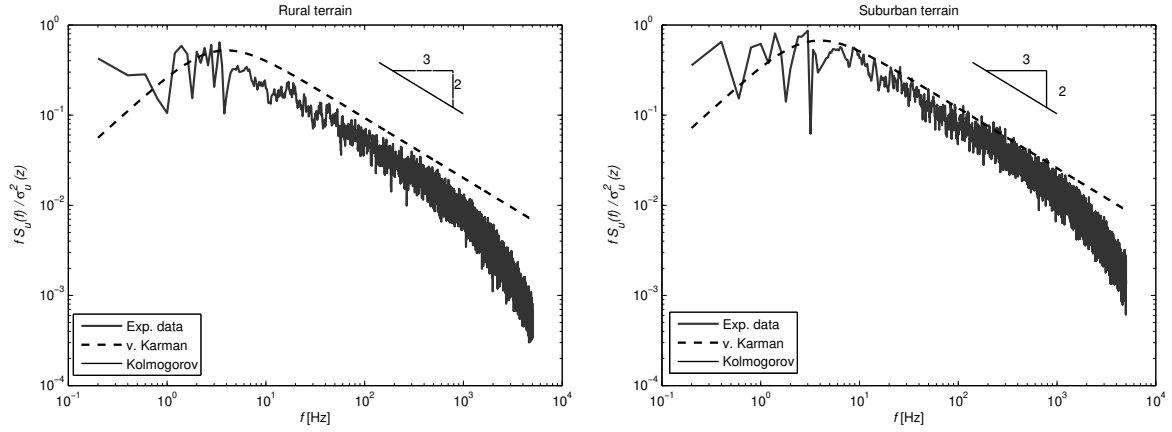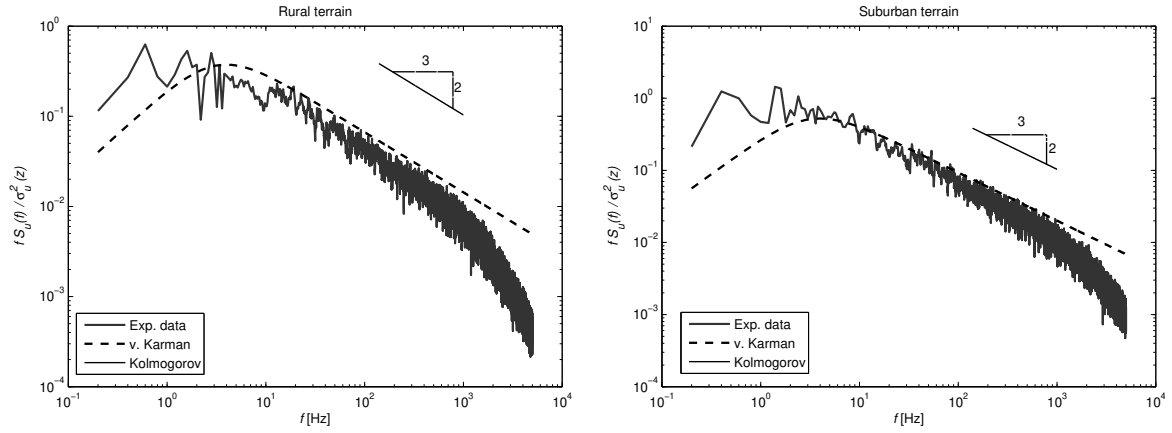
4.2.1.   Stand-alone building

Time intervals between an opening and closing the windows were set to 3 and 5 s. Measurements were carried out in series from the starting concentrations of around 50% $(\frac{m_{CO_2}}{m_{CO_2}+m_{air}})$ to the final of around 10%. The ACH for each point was calculated as an average of several measurements. After computing the simulation length scale factor, the ACH was scaled. Figure 4.13 represents the influence of the flow incidence angle on the ACH for a single-side ventilation. The same effect, but for cross ventilation, is shown in Fig. 4.14.

Figure 4.13: Air change rate (ACH) for various flow incidence angles for a single-side ventilation of a stand-alone cubic building model

In a single-side ventilated stand-alone building model there is no significant difference between the ACH values for different terrain types. The ACH is at the maximum for an incidence angle $\beta = 90°$. The flow in the perpendicular direction to the opening creates a lower pressure region near the window. The created pressure gradient between the

interior space and the external flow sucks the air outwards. At the angles of $\beta = 0°$ and $\beta = 180°$ the stagnation point is created in front of the window. This prevents the air change with the environment and reduces the ACH. That is not the case for the cross-ventilated space.

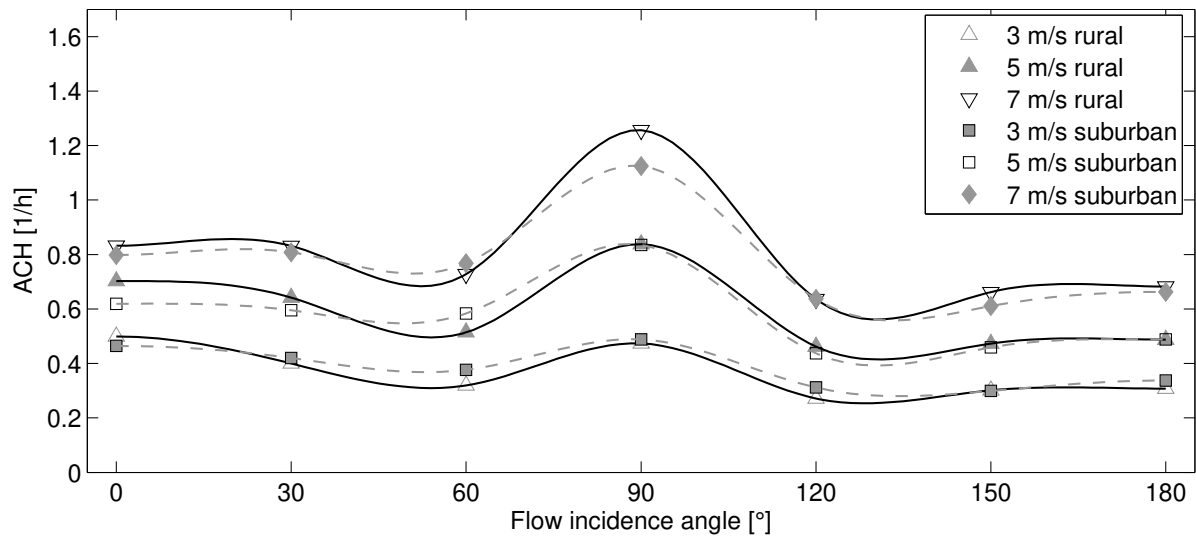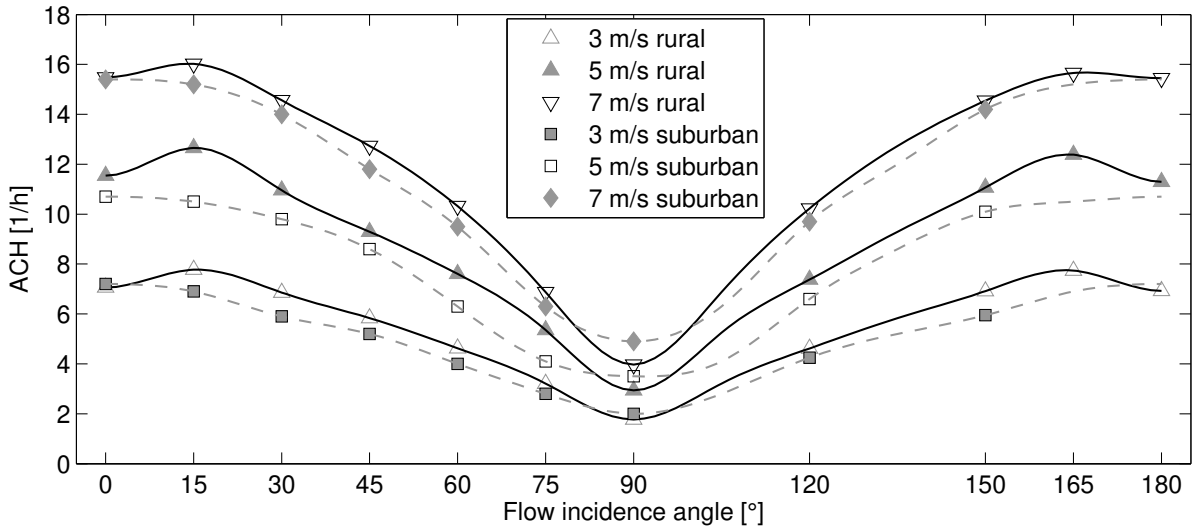

Figure 4.14: Air change rate (ACH) for various flow incidence angles for a cross ventilation of a stand-alone cubic building model

For the cross-ventilated space, the flow enters the model through the front window and exits through the rear window. That way a substantial amount of air circulates through the indoor space. In the cross ventilated spaces, the ACH is largest for $\beta = 0°$. As the flow incidence angle increases, the ACH decreases. The minimum is reached at the incidence angle $\beta = 90°$. The results for the rural and suburban ABL simulation have similar trends. The largest difference is that for the suburban ABL simulation the peak value is around $\beta = 0°$, while for the rural ABL simulation it is around $\beta = 15°$. Further analysis of Figs. 4.13 and 4.14 reveals that the values of the ACH for cross ventilation are significantly larger. The ACH for the cross-ventilated stand-alone building model is from 2 to 16 h^{-1}, while for the single-side ventilation it is from 0.25 to 1.25 h^{-1}. An increase in the flow velocity yields an increase of the ACH.

4.2.2. Building natural ventilation in an urban neighbourhood

The ACH was measured for three test cases, i.e. a) $d = 100$ mm $= 0.5a$, b) $d = 200$ mm $= a$ and c) $d = 300$ mm $= 1.5a$. The effects of the spacing density among the building models, flow incidence angle and velocity were studied.

Single-side ventilation

The ACH dependence on the flow incidence angle for a single-side ventilation is shown in Figs. 4.15, 4.16 and 4.17. Measurements were carried out for $\beta = 0°$ to $\beta = 180°$. The trends and values of the ACH for $\beta = 180° - 360°$ are the same as for $\beta = 0°$ to $\beta = 180°$ due to symmetry.
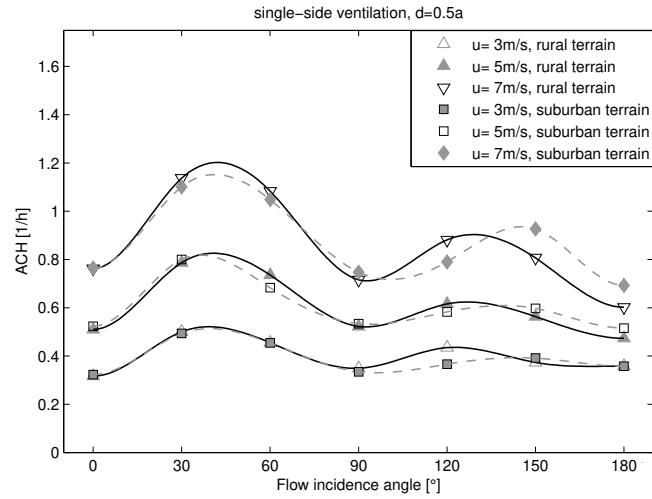
Figure 4.15: Air Change Rate (ACH) for various flow incidence angles for the cubic building model as a part of a group of buildings, single-side ventilation case a)
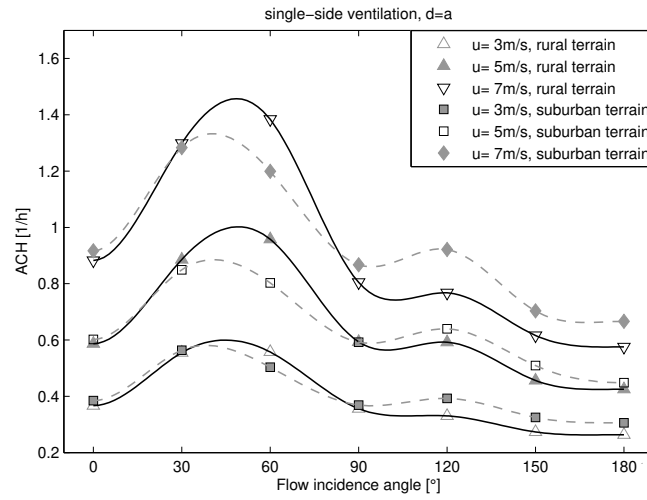
Figure 4.16: Air Change Rate (ACH) for various flow incidence angles for the cubic building model as a part of a group of buildings, single-side ventilation case b)
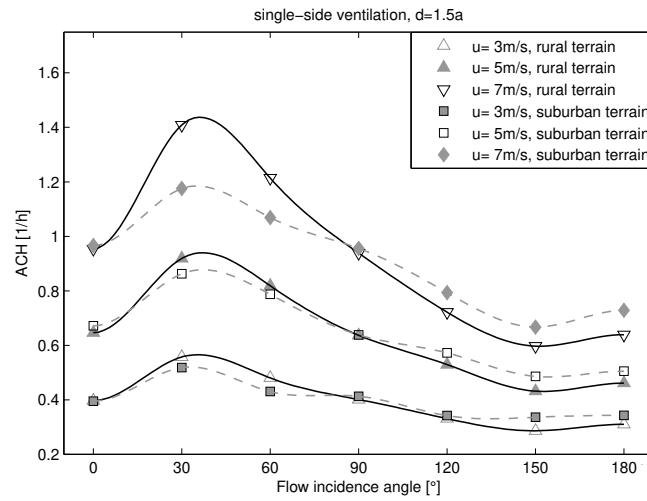
Figure 4.17: Air Change Rate (ACH) for various flow incidence angles for the cubic building model as a part of a group of buildings, single-side ventilation case c)

There is a clear difference in the ACH behaviour between the stand-alone building model and the one situated in the neighbourhood. When the building is surrounded by other buildings, the peak values shift from $\beta = 90°$ to smaller flow incidence angles. The maximum is reached between 30° and 60°. Golubić [37] noticed that the reason for that phenomenon might be a gap between the building models. These gaps are passages that enable the flow to pass through the building opening and directly enhance the

ventilation. It is interesting that the peak ACH values for the b) and c) cases are larger than for a stand-alone building model. The a) case reveals another trend. The gap between the building models is too small, and the air flow is blocked. Figure 4.18 shows these passages for the c) and a) cases. The first one does not allow a large amount of air to pass between the buildings. Nevertheless, the air that "manages" to pass through the tight passage is accelerated due to a reduced cross-section for the flow. The static pressure drops and the flow velocity is increased. The result is a larger air suction from the inside out. That is why the peak value of the a) case remained the same, while for other cases it increased.
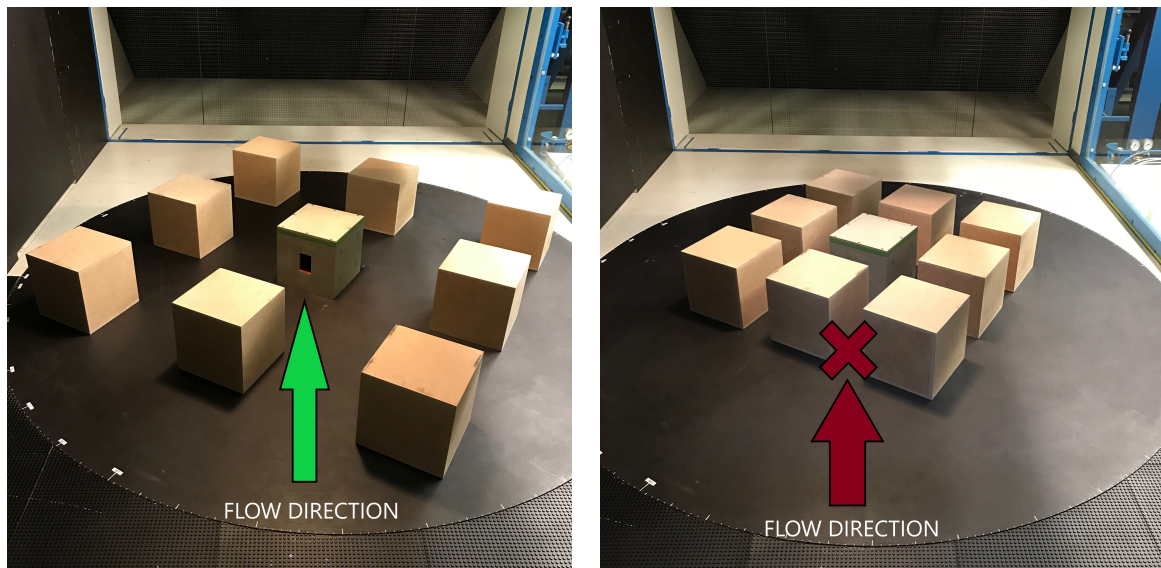
Figure 4.18: Passage between models in 3x3 square pattern. Left is case c), right case a)

It is interesting to note that the trends for the rural and suburban ABL simulations are quite similar. The most significant difference is that the rural ABL simulation is more sensitive to changes in the flow incidence angle. For a given velocity and spacing density it reaches both the maximum and minimum values, while the suburban ABL simulation is less sensitive.

The ACH for various spacing densities at the constant flow incidence angle impinging the building model situated in the urban neighbourhood model is presented in Fig. 4.19.
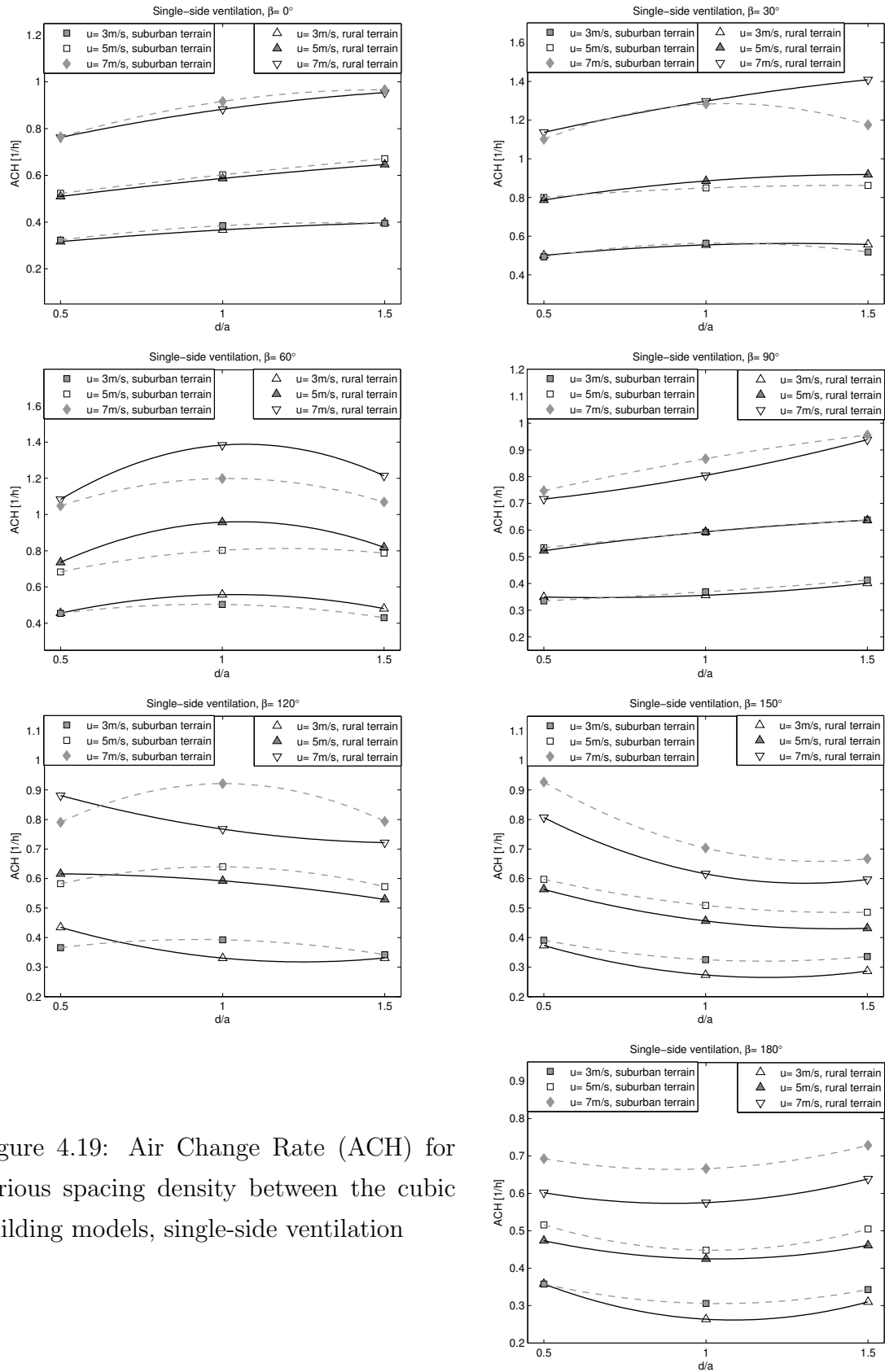
Figure 4.19: Air Change Rate (ACH) for various spacing density between the cubic building models, single-side ventilation

In the range from $\beta = 0°$ to $\beta = 30°$ the ACH increases with increasing d. The exceptions are high speeds in the suburban ABL simulation at $\beta = 30°$. The curves for $\beta = 90°$ and $\beta = 180°$ are almost flat and a mild drop with increasing spacing density is observed at $\beta = 150°$. In the rural ABL simulation the trends are generally similar but more exhibited.

Cross ventilation

The cross-ventilation results are reported in Figs. 4.20 to 4.22 from $\beta = 0°$ to $\beta = 90°$.
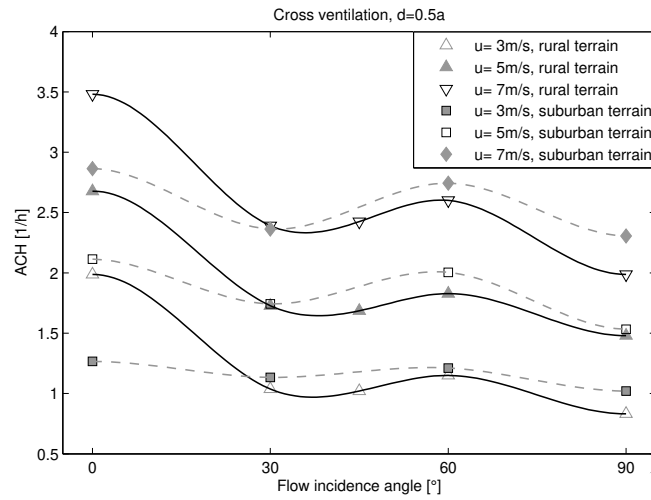
Figure 4.20: Air Change Rate (ACH) for various flow incidence angles for the cubic building model as a part of a group of buildings, cross ventilation case a)
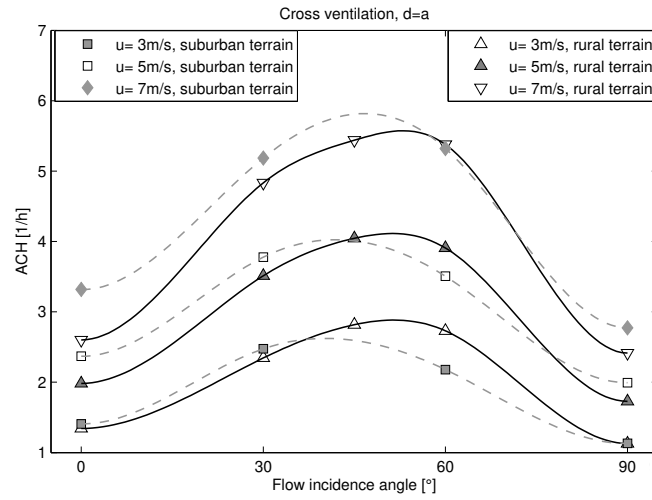
Figure 4.21: Air Change Rate (ACH) for various flow incidence angles for the cubic building model as a part of a group of buildings, cross ventilation case b)
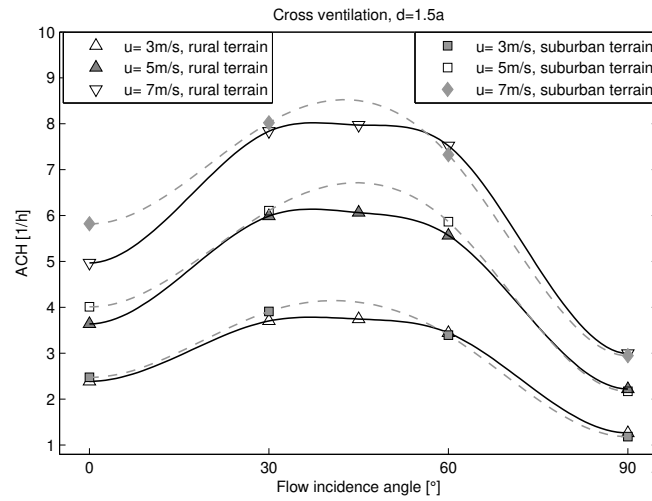
Figure 4.22: Air Change Rate (ACH) for various flow incidence angles for the cubic building model as a part of a group of buildings, cross ventilation case c)

The results differ substantially depending on the passage width among the building models. For the a) case, where the flow cross-section is minimal, the peak ACH value is also minimal compared to other cases. It is located at $0°$. There is a drop in the ACH toward $\beta = 30°$ followed by another small growth till $\beta = 60°$. The minimal value of the ACH is at $90°$. For the b) and c) cases, the maximum is shifted to the larger flow incidence angles. This may be due to the ability of the free flow to easier approach the

entrance to the building model. The maximum ACH is around 8.5 h^{-1} for $d = 1.5a$ at the velocity of 7 m/s, which is still just a half of the ACH obtained for the stand-alone building model. The ACH is larger at larger incident flow velocities. While the ACH trends for the rural and suburban ABL simulations are quite similar, the gradients in the rural ABL simulation are more exhibited. Figure 4.23 shows the ACH as a function of various spacing densities for both terrains. The flow incidence angles were the same and results are presented for $\beta = 0, 30, 60$ and $90°$.

Figure 4.23: Air Change Rate (ACH) for various spacing density between buildings, cross ventilation

5 | Conclusion

Small-scale experiments were carried out to investigate the influence of wind characteristics on the natural ventilation of buildings. The inflow conditions impinging the building model were the wind-tunnel simulations of the atmospheric boundary layers (ABLs) developing above the rural and suburban type terrains. The building model was a wall-mounted cube. The ventilation effic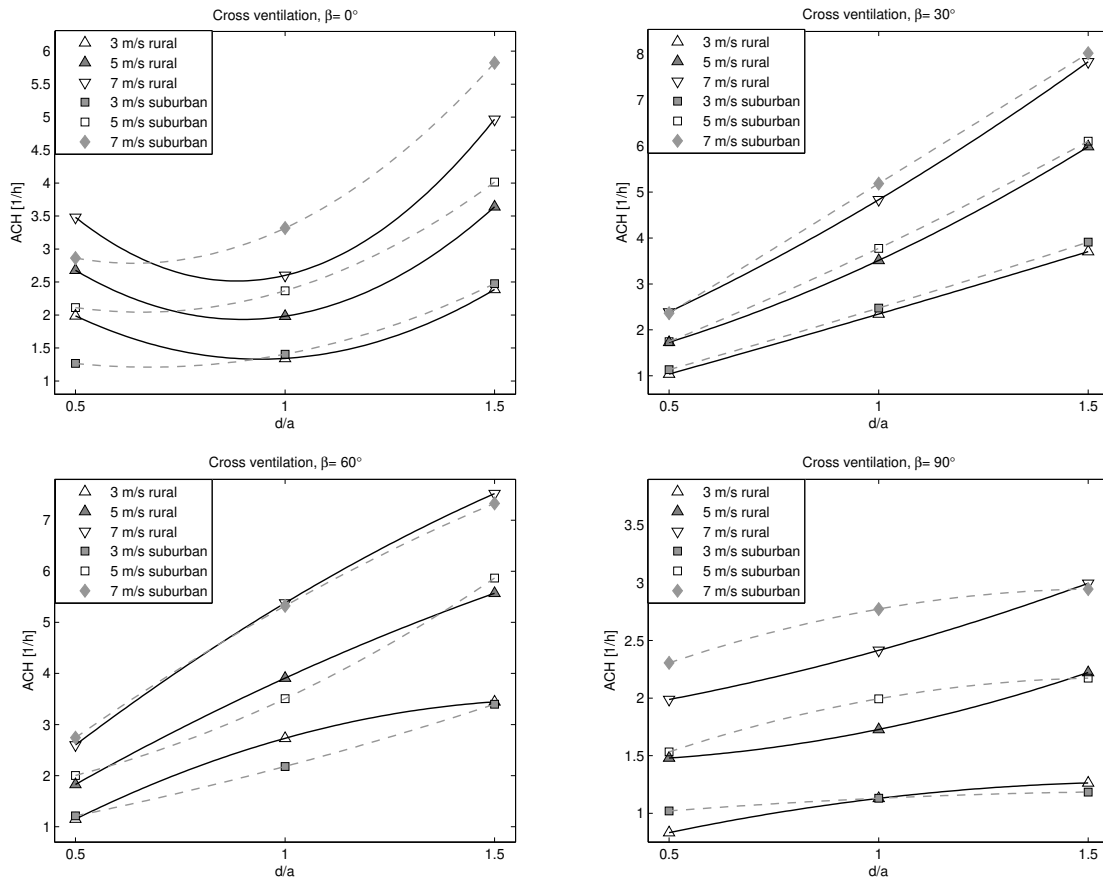iency was studied for a stand-alone building model and for a building model situated in a model of a generic urban neighborhood. The experiments were performed for one and two windows on the building model placed at various flow incidence angles β.

The hot-wire anemometry system was used to determine flow characteristics. The natural ventilation was quantified by measuring the Air Change Rate (ACH) using the tracer gas system. The experiments were conducted in a boundary layer wind tunnel of the Institute of Fluid Mechanics and Heat Transfer at the Graz University of Technology, Austria.

The velocity profiles correspond well to the power-law with the exponent of $\alpha = 0.22$ for the suburban and $\alpha = 0.15$ for the rural type terrains. The logarithmic law components z_0 and u_τ agree with the values recommended in the international Engineering Sciences Data Unit (ESDU) standard. Turbulence intensities for a flow over suburban area show a good agreement with the ESDU 85020 in a lower region of the ABL simulation, while for the rural ABL simulation those values are rather small. The measurements verified the inability of integral turbulence length scales to fully develop in a wind tunnel, which is a well-known problem. The Reynolds shear stress is close to the zero near the ground and approximately constant throughout the inertial sublayer

in agreement with the atmospheric conditions. The power spectral density of velocity fluctuations compares well with the theoretical models of von Kármán and Kolmogorov.

Single-side ventilation measurements of a stand-alone building model showed maximal values of the ACH for $\beta = 90°$. The flow perpendicular to the opening in the building creates the suction on the sidewalls façade that sucks the inside air out of the room. In the building model surrounded by other objects this effect can be amplified due to the reduced cross-section for the flow, i.e. an increase in the velocity. On the other hand, the peak values of the ACH for cross-ventilated stand-alone object were observed for $\beta = 0°$ and $\beta = 15°$ for the suburban and rural ABL simulations, respectively. The trends observed are quite similar for both studied terrain types. Nevertheless, a clear discrepancy is that the rural ABL flow is more sensitive to the changes in the flow incidence angle.

Bibliography

[1] B. Langensteiner. *Transport processes in ventilated buildings.* PhD thesis, Technische Universität Graz, 2014.

[2] C. Allocca, Q. Chen, L. R. Glicksman. Design analysis of single-sided natural ventilation. *Energy and Buildings*, 2003.

[3] G. M. Stavrakakis, M. K. Koukou, M. Gr. Vrachopoulos, and N. C. Markatos. Natural cross-ventilation in buildings: Building-scale experiments, numerical simulation and thermal comfort evaluation. *Energy and Buildings*, 2008.

[4] D. Ernest, F. Bauman, and E. Arens. The effects of external wind pressure distributions on wind-induced air motion inside buildings. *Journal of Wind Engineering and Industrial Aerodynamics*, 1992.

[5] O. P. Cheung and C. H. Liu. CFD simulations of natural ventilation behaviour in highrise buildings in regular and staggered arrangements at various spacings. *Energy and Buildings*, 2011.

[6] B. Lee, M. Hussain, and B. Soliman. A method for the assessment of the wind induced natural ventilation forces acting on low rise building arrays. *Building Services Engineering Research and Technology*, 2011.

[7] T. R. Oke. *Boundary layer climates.* Taylor & Francis e-Library, 2002.

[8] W. Wang and E. Ng. Air ventilation assessment under unstable atmospheric stratification - A comparative study for Hong Kong. *Building and Environment*, 2018.

[9] W. H. Hucho. Aerodynamik stumpfer Körper. Physikalische Grundlagen und An-
     wendungen in der Praxis. *Vieweg Braunschweig/Wiesbaden*, 2013.

[10] C. Dyrbye and S. O. Hansen. Wind loads on structures. *John Wiley and Sons,
     London*, 1997.

[11] H. Kozmar. *Utjecaj mjerila na strukturu modeliranog atmosferskog graničnog sloja.*
     PhD thesis, University of Zagreb, 2005.

[12] R. H. Thuiller and U. O. Lappe. Wind and Temperature Profíle Characteristics
     from Observations on a 1400 ft Tower. *Journal of Applied Meteorology*, 1964.

[13] *WTG: Windkanalversuche in der Gebäudeaerodynamik, Windtechnologische
     Gesellschaft WTG e.V., 1994.*

[14] *ESDU: Characteristics of wind speed in the lower layers of the atmosphere near the
     ground: strong winds (neutral atmosphere), 72026, 1972.*

[15] T. Likso. Estimation of Wind Speed in the Suburban Atmospheric Surface Layer.
     Presentation for Meteorological and Hydrological Service, Zagreb, Croatia.

[16] J. Wieringa, A. Davenport, C. Grimmond, and T. Oke. New revision of Davenport
     roughness classification. Proceedings of the 3rd European and African Conference
     on Wind Engineering. In *Eindhoven*, 2001.

[17] *A. Pernpeintner : Lecture notes from course: "Aerodynamik der Bauwerke",
     Lehrstuhl für Fluidmechanik, Fakultät für Maschinenwesen, TU-München, 1998.*

[18] H. Kozmar. Physical modeling of complex airflows developing above rural terrains.
     Environmental Fluid Mechanics, 2012.

[19] H. Kozmar. Truncated vortex generators for part-depth wind-tunnel simulations of
     the atmospheric boundary layer flow. *Journal of Wind Engineering and Industrial
     Aerodynamics*, 2011.

[20] H. Kozmar. Characteristics of natural wind simulations in the TUM boundary layer
     wind tunnel. *Theoretical and Applied Climatology*, 2011.

[21] *ESDU, Engineering Sciences Data Unit, 74031, Characteristics of atmospheric turbulence near the ground, Part II: single point data for strong winds (neutral atmosphere), 1975.*

[22] J. C. Wyngaard. Atmospheric turbulence. *Annual Review of Fluid Mechanics*, 1992.

[23] B. S. Taranath. *Structural Analysis and Design of Tall Buildings: Steel and Composite Construction* . CRC Press, 2012.

[24] J. Counihan. Adiabatic atmospheric boundary layers: A review and analysis of data from the period 1880-1972. *Atmospheric Environment*, 1975.

[25] *TSI Manual: Turbulence Intensity Measurements Application Note AF-141.*

[26] H. Sockell. Aerodynamik der Bauwerke. *Vieweg & Sohn*, 1984.

[27] *NPTEL: National Programme on Technology Enhanced Learning - Lecture notes.*

[28] J. Garratt. The atmospheric boundary layer. *Cambridge University Press*, 1992.

[29] H. Kozmar. Industrial aerodynamics. *Material for lectures*, 2017.

[30] R. Martinuzzi C. Tropea. The flow around surface-mounted, prismatic obstacles placed in a fully developed channel flow. *Trans. ASME, J. Fluid Eng*, 1993.

[31] R. Martinuzzi, H. Hussein. Energy balance for turbulent flow around a surface mounted cube placed in a channel. *Phys. Fluids 8 (3), 764–780.*, 1996.

[32] M. F. P. Lopez. Numerical calculation of the wind action on buildings using Eurocode 1 atmospheric boundary layer velocity profiles. *Wind and Structures*, 2010.

[33] Y. T. Lee, S. Boo, H. Chang Lim and K. Misutani. Pressure distribution on rectangular buildings with changes in aspect ratio and wind direction. *Wind and Structures, Vol. 23, No. 5*, 2016.

[34] A. Kubilay. Wind flow around 9 staggered cubes. Technical report, ETH Zurich, 2019.

[35] M. F. King, H. L. Gough, C. Halios, J. F. Barlow, A. Robertson, R. Hoxey, C. J.Noakesa. Investigating the influence of neighbouring structures on natural ventilation potential of a full-scale cubical building using time-dependent CFD. *Journal of Wind Engineering and Industrial Aerodynamics*, 2017.

[36] I. Castro, Z. Xie, V. Fuka, A.G. Robins, M.Carpentieri, P. Hayden, D. Hertwig, O. Coceal. Measurements and computations of flow in an urban street system. *Boundary-Layer Meteorology*, 2017.

[37] D. Golubić. Experimental model of building natural ventilation in urban environment. Master's thesis, Faculty of Mechanical Engineering and Naval Architecture, University of Zagreb, 2018.

[38] J. O. Hinze. *Turbulence*. McGraw-Hill Collage, 1975.

[39] *Dantec Dynamics, "Probes for Hot-wire Anemometry" , catalogue, 2015.*

[40] F. E. Jorgensen. How to measure turbulence with hot-wire anemometers - a practical guide. *Dantec Dynamics*, 2005.

[41] *LumaSense Technologies, Instruction Manual, INNOVA -1316A-2 Multi Gas Monitor, 2011.*

[42] E. Choi. Proposal for unified terrain categories exposures and velocity profiles. In *The Seventh Asia-Pacific Conference on Wind Engineering, Taipei, Taiwan*, November 8-12, 2009.

[43] N. J. Cook. Determination of the model scale factor in wind tunnel simulations of the adiabatic atmospheric boundary layer. *Journal of Wind Engineering and Industrial Aerodynamics*, 1978.

[44] A. Yakhot, H. Liu, N. Nikitin. Turbulent flow around a wall-mounted cube: A direct numerical simulation. *International Journal of Heat and Fluid Flow 27*, 2006.

[45] S. Dudek I. Abohela, N. Hamza. Validating CFD simulation results: Wind flow around a surface mounted cube in a turbulent channel flow. *PLEA2012 - 28th Conference, Opportunities, Limits & Needs Towards an environmentally responsible architecture Lima, Perú*, 2012.

[46] *ESDU, Engineering Sciences Data Unit, 85020, "Characteristics of atmospheric turbulence near the ground, Part II: single point data for strong winds (neutral atmosphere)," 1985.*